VLT Spectroscopy of Ultra-Faint Dwarf Galaxies. 1. Boötes I, Leo IV, Leo V

Sydney Jenkins,[1] Ting S. Li,[2,3,4,*] Andrew B. Pace,[5] Alexander P. Ji,[2] Sergey E. Koposov,[6,7] and
Burçin Mutlu-Pakdil[8,9]

[1]Department of Physics, University of Chicago, Chicago, IL 60637, USA
[2]Observatories of the Carnegie Institution for Science, 813 Santa Barbara St., Pasadena, CA 91101, USA
[3]Department of Astrophysical Sciences, Princeton University, Princeton, NJ 08544, USA
[4]Department of Astronomy and Astrophysics, University of Toronto, 50 St. George Street, Toronto ON, M5S 3H4, Canada
[5]McWilliams Center for Cosmology, Carnegie Mellon University, 5000 Forbes Ave, Pittsburgh, PA 15213, USA
[6]Institute for Astronomy, University of Edinburgh, Royal Observatory, Blackford Hill, Edinburgh EH9 3HJ, UK
[7]Institute of Astronomy, University of Cambridge, Madingley Road, Cambridge CB3 0HA, UK
[8]Kavli Institute for Cosmological Physics, University of Chicago, Chicago, IL 60637, USA
[9]Department of Astronomy and Astrophysics, University of Chicago, Chicago, IL 60637, USA

ABSTRACT

We perform consistent reductions and measurements for three ultra-faint dwarf galaxies (UFDs): Boötes I, Leo IV and Leo V. Using the public archival data from the GIRAFFE spectrograph on the Very Large Telescope (VLT), we locate new members and provide refined measurements of physical parameters for these dwarf galaxies. We identify nine new Leo IV members and four new Leo V members, and perform a comparative analysis of previously discovered members. Additionally, we identify one new binary star in both Leo IV and Leo V. After removing binary stars, we recalculate the velocity dispersions of Boötes I and Leo IV to be $5.1^{+0.7}_{-0.8}$ and $3.4^{+1.3}_{-0.9}$ km s^{-1}, respectively; We do not resolve the Leo V velocity dispersion. We identify a weak velocity gradient in Leo V that is ∼4× smaller than the previously calculated gradient and that has a corresponding position angle which differs from the literature value by ∼120 deg. Combining the VLT data with previous literature, we re-analyze the Boötes I metallicity distribution function and find that a model including infall of pristine gas while Boötes I was forming stars best fits the data. Our analysis of Leo IV, Leo V and other UFDs will enhance our understanding of these enigmatic stellar populations and contribute to future dark matter studies. This is the first in a series of papers examining thirteen UDFs observed with VLT/GIRAFFE between 2009 and 2017. Similar analyses of the remaining ten UFDs will be presented in forthcoming papers.

1. INTRODUCTION

The population of known Local Group galaxies has grown steadily in the past two decades with the discovery of many new ultra-faint dwarf (UFD) galaxies (e.g., Belokurov et al. 2006, 2007, 2008; Bechtol et al. 2015; Koposov et al. 2015a; Mau et al. 2020). Characterized by an older stellar population, low metallicity, and low surface brightness, UFDs are the most dark-matter dominated systems known (Simon & Geha 2007;

Gilmore et al. 2007; Simon 2019) and may play a key role in characterizing dark matter. For instance, UFD central densities can be used to test dark matter models (e.g., Calabrese & Spergel 2016) and the number of Milky Way dwarf galaxy satellites can be used to constrain the mass of warm dark matter particles (Kennedy et al. 2014; Nadler et al. 2020). Additionally, their compactness and proximity make them ideal sites for indirect dark matter detection (e.g., Ahnen et al. 2018; Hoof et al. 2020).

The characteristics of individual stars within a UFD can be used to understand the global properties of the galaxy (e.g., Simon & Geha 2007). For example, the velocities of member stars can constrain dynami-

Corresponding author: Sydney Jenkins, Ting S. Li
sydneyjenkins@uchicago.edu, tingli@carnegiescience.edu

* NHFP Einstein Fellow

cal mass and dark matter content. However, due to their low luminosity, many UFDs have few known member stars, making it difficult to provide robust measurements of the galaxies' key features. To better constrain UFDs' kinematic and metallicity parameters, we uniformly reduce and analyze archived data from the FLAMES/GIRAFFE spectrograph on the Very Large Telescopes (VLT) for thirteen UFDs. In this study, we present our membership selection process and results for three UFDs: Boötes I, Leo IV and Leo V. Boötes I data from VLT has been previously published (Koposov et al. 2011) and is used here to validate our data reduction and membership selection processes. Our membership analysis of the remaining ten UFDs observed with VLT/GIRAFFE will be presented in a follow-up study.

Boötes I, Leo IV and Leo V were discovered as stellar overdensities in Sloan Digital Sky Survey (SDSS) data (Belokurov et al. 2006, 2007, 2008). Boötes I is one of the more luminous UFDs ($M_V = -6.0$, Muñoz et al. 2018). Photometric studies show that Boötes I is dominated by ancient metal-poor populations (Brown et al. 2014), and spectroscopic studies have provided insight into the stellar kinematics and chemical abundances of Boötes I (Muñoz et al. 2006; Martin et al. 2007; Wolf et al. 2010; Norris et al. 2010; Koposov et al. 2011; Lai et al. 2011). Additionally, Koposov et al. (2011) presented evidence for a two-population kinematic model, with the higher dispersion component concentrated closer to the center of the dwarf galaxy. The authors suggest that this may reflect the UFD's formation, which potentially involved the merging of several smaller populations.

Simon & Geha (2007) used medium-resolution spectroscopy to identify 18 members stars in Leo IV and found a velocity dispersion of 3.3±1.7 km s^{-1}. A follow-up analysis by Kirby et al. (2013) found that Leo IV has a metallicity of $-2.29^{+0.19}_{-0.22}$ dex and an internal metallicity spread of $0.56^{+0.19}_{-0.14}$ dex. Muñoz et al. (2018) have refined calculations of Leo IV's size ($r_h = 114\pm13$ pc) and magnitude ($M_V = -4.99^{+0.26}_{-0.26}$).

Leo V is close to Leo IV in both location and radial velocity, with separations of 0.3 degrees and 50 km s^{-1}, respectively. These similarities have motivated investigations into their possible relationship (e.g., de Jong et al. 2010; Blaña et al. 2012)). Additionally, several spectroscopic studies have targeted Leo V. Walker et al. (2009) identified seven likely members, two of which are more than ten half-light radii away from Leo V's center. Collins et al. (2017) found an additional five members, and also presented tentative evidence of a velocity gradient (-4.1$^{+2.8}_{-2.6}$ km s^{-1} per arcmin). They argue that this gradient, angled toward the Milky Way center, might suggest that Leo V is on the verge of dissolution follow-

ing a close encounter with the Milky Way. Using their membership catalogue, they calculated a velocity dispersion of $2.3^{+3.2}_{-1.6}$ km s^{-1}. Mutlu-Pakdil et al. (2019) assessed both spectroscopic studies using high-precision photometry, spectra, and *Gaia* measurements. They concluded that the debris stream identified by Sand et al. (2012) is composed of background galaxies and foreground stars and that the velocity gradient found by Collins et al. (2017) may be due to small number statistics.

We locate member stars in Boötes I, Leo IV and Leo V using public spectroscopic data from the Very Large Telescope (VLT). The archive data were collected with the GIRAFFE spectrograph and FLAMES fiber positioner. We describe the data and data reduction in §2 and perform velocity and metallicity measurements in §3. The analyses in both §2 and §3 are applied to all thirteen UFDs listed in Table 1, which were observed by GIRAFFE/FLAMES between 2009 and 2017. In §4, we identify members stars in Boötes I, Leo IV and Leo V. We then discuss our membership results and present our updated physical parameter values in §5 before concluding in §6.

2. OBSERVATIONS AND DATA REDUCTION

2.1. *VLT Data*

We use the publicly available data from the ESO science archive facility[1]. Table 1 lists the thirteen UFDs that were observed by FLAMES/GIRAFFE (Pasquini et al. 2000) between 2009 and 2017 using the LR8 grating and covering the wavelength range from 8206 - 9400 Å at a spectral resolution of $R \sim 6,000$. Most of these data were unpublished at the start of this project. Notably, Boötes I spectroscopy was presented by Koposov et al. (2011), and we use it here to validate our results.[2] For most UFDs, one field was observed repeatedly to obtain the desired signal-to-noise ratio (S/N) and detect binaries.

We uniformly reduce the data and calculate radial velocity and metallicity measurements for all UFDs listed in Table 1. In this paper, we only perform membership selection for Boötes I, Leo IV and Leo V. We use 21 exposures of Boötes I, with 20 exposure times between 45 and 58 minutes and one exposure time of 27 minutes. Boötes I observations took place between February and March 2009. We use 17 exposures of Leo IV of approximately 45 minutes each. These observations took place

---

[1] https://archive.eso.org/eso/eso_archive_main.html

[2] Fritz et al. (2019) also used the archived VLT data to study several UFDs. A comparison with their measurements will be discussed in a future paper.

Table 1. VLT Ultra-Faint Dwarf Galaxies

UFD	Proposal ID(s)	Time	$N_{\rm exp}$	$T_{\rm exp}$ (s)	NStars	Kinematic Studies
Boötes I	182.B-0372(A)	2/2009-3/2009	21	59350	118	Muñoz et al. (2006), Martin et al. (2007), Lai et al. (2011), Koposov et al. (2011)
Leo IV	185.B-0946(A)	5/2010-3/2011	17	45700	104	Simon & Geha (2007)
Leo V	185.B-0946(B)	5/2010-3/2011	17	46100	105	Walker et al. (2009), Collins et al. (2017), Mutlu-Pakdil et al. (2019)
Columba I	098.B-0419(A)	12/2016	6	16650	76	Fritz et al. (2019)
Eridanus II	096.B-0785(A)	11/2015-12/2015	4	12000	110	Li et al. (2017), Zoutendijk et al. (2020)
Grus I	096.B-0785(A)	10/2015-11/2016	4	8940	114	Walker et al. (2016)
Horologium I	096.B-0785(A)	10/2015-10/2016	4	10980	114	Koposov et al. (2015b)
	096.D-0967(B)	12/2015-1/2016	14	38850	110	
Horologium II	098.B-0419(A)	12/2016-2/2017	3	8325	115	Fritz et al. (2019)
Phoenix II	096.B-0785(A)	6/2016-9/2016	4	10980	105	Fritz et al. (2019)
Reticulum II	096.B-0785(A)	10/2015-10/2016	6	11880	114	Walker et al. (2015), Simon et al. (2015), Koposov et al. (2015b)
Reticulum III	098.B-0419(A)	12/2016-2/2017	3	8325	75	Fritz et al. (2019)
Segue 1	185.B-0946(G)	3/2011-6/2012	17	19110	114	Simon et al. (2011), Geha et al. (2009)
	185.B-0946(F)	4/2011-6/2012	17	21580	116	
Tucana II	096.B-0785(A)	12/2015-10/2016	4	10980	115	Walker et al. (2016), Chiti et al. (2018), Chiti et al. (2020)
	096.D-0967(A)	10/2015	2	4890	114	

in two groups approximately eight months apart (May to July 2010 and February to March 2011). We similarly use 17 exposures of Leo V, all of approximately 45 minutes. These observations took place in two groups approximately seven months apart (July 2011 and January to March 2012).

2.2. Data Reduction

We reduce the raw science data associated with the studies listed in Table 1 using the GIRAFFE Gasgano pipeline[3], which provides bias subtraction, flat-fielding, wavelength calibration and 1D spectral extraction. To minimize the fiber-dependent radial velocity offsets observed in Koposov et al. (2011), the resulting spectra from each exposure are re-calibrated using sky emission lines from Hanuschik (2003). A total of 12 relatively strong and isolated sky lines between 8340 Å and 8950 Å are used in this re-calibration. We fit a linear relation between the measured wavelength λ' and the literature value of the sky emission lines λ:

$$\frac{\lambda' - \lambda}{\lambda} c = a_1 \times \frac{\lambda - 8600\text{Å}}{200\text{Å}} + a_0 \qquad (1)$$

where c is the speed of light, a_0 is the shift in $\rm km\,s^{-1}$ at 8600 Å (zero-order shift), and a_1 is the shift for every 200 Å from 8600 Å (the first-order shift). We then fit a six-degree polynomial to the zero and first-order shifts as a function of fiber number and apply the shift from the polynomial fit to each spectra. Examples of the shifts are given in Figure 1, where we show the zero and first order shifts for two exposures of Leo IV and Leo V. Trends in the zero and first order shifts vary between exposures and UFDs.

We perform sky subtraction by selecting the sky fibers in each observation and averaging them to produce a master sky spectrum. The master sky spectrum is then

[3] http://www.eso.org/sci/software/gasgano.html

scaled to match the amplitude of the bright, isolated sky lines of each fiber before being subtracted from the science spectrum. We combine the individual exposures using inverse-variance weighting, creating a combined spectrum for each star. Example spectra ranging from low to high S/N are provided in Figure 2.

To obtain parallax and proper motion data, we cross-match the VLT stars with *Gaia* EDR3 (Gaia Collaboration et al. 2016; Collaboration et al. 2020) by identifying the nearest neighbor for each VLT source with separation < 1". We similarly cross-match the VLT stars with the Dark Energy Camera Legacy Survey (DECaLS) DR8 (Dey et al. 2019) to obtain photometric data. All photometric data reported in this paper are reddening corrected using extinction map from Schlegel et al. (1998). The proper motion and photometric data are then combined with the VLT data to form a joint catalogue of stars. In this paper, we use the IDs in the raw science data to distinguish stars, with the exception of stars in Boötes I; for Boötes I, we label stars by appending the ID from Koposov et al. (2011) to the prefix "Boo1."

3. VELOCITY AND METALLICITY MEASUREMENTS

3.1. Radial Velocity Measurements

To determine the heliocentric radial velocities $\rm v_{hel}$ of each star, we use the template-fitting code described in Li et al. (2017). Because no velocity standard stars were observed with VLT, and the Keck/DEIMOS spectra have a much wider wavelength coverage and a similar resolution ($R \sim 6,000$) as the VLT spectra, we use a list of Keck/DEIMOS templates from Kirby et al. (2015) that are shifted to zero velocity based on their known velocities. These stellar templates have various effective temperatures, surface gravities, and metallicities, and are fit to the observed spectra using a Markov Chain Monte Carlo (MCMC) sampler (Foreman-Mackey et al. 2013). We adopt a uniform radial velocity prior be-
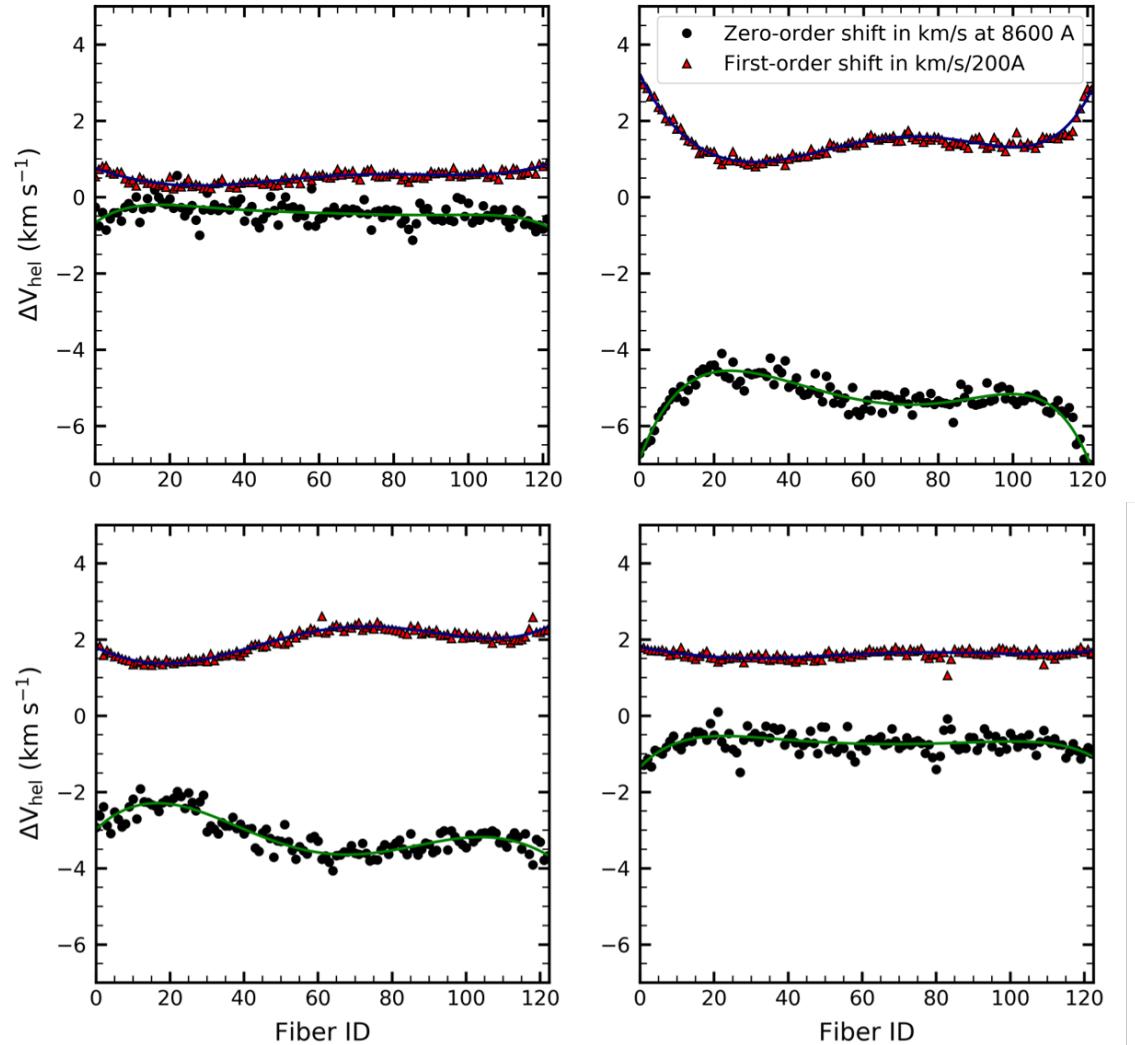
Figure 1. Examples of the shifts in wavelength recalibration using sky emission lines as a function of fiber ID for each GIRAFFE exposure. The green and blue curves represent sixth degree polynomial fits to the zero and first-order shifts, respectively. We apply the shift corresponding to the polynomial fit to each spectra. Top: Two observations of Leo IV. Bottom: Two observations of Leo V.

tween ± 800 km s^{-1} and use a 100-iteration burn-in to initialize our sampler. The radial velocity posterior distribution is sampled using the ensemble sampler `emcee` with 20 walkers and 900 iterations. We then use the median and standard deviation of the posterior chain to compute the radial velocity and radial velocity error, respectively, for each template. We select the radial velocity and error values corresponding to the template fit with the lowest chi-squared value. The radial velocity uncertainties are underestimated and adjusted accordingly (see §3.2).

We apply several quality checks to our radial velocity results. We use a Random Forest classifier (RFC), as in Li et al. (2019), to identify spectra that do not corre-

spond to stars or good fits. Because the calculated radial velocity of non-stellar or low quality spectra are often large—near the upper and lower limits of the allowed ± 800 km s^{-1} range—we classify any star with an absolute radial velocity greater than 500 km s^{-1} as a poor fit. We then train the RFC using the reduced chi-squared, S/N, absolute deviation, velocity skew, kurtosis and uncertainty of each velocity measurement as features. We apply our trained RFC to the VLT data, providing us with the probability that each star is a good stellar spectrum. We classify all observations with a probability less than 0.6 as bad fits and create a corresponding binary good_star flag that is set to one for good fits and zero for bad fits.
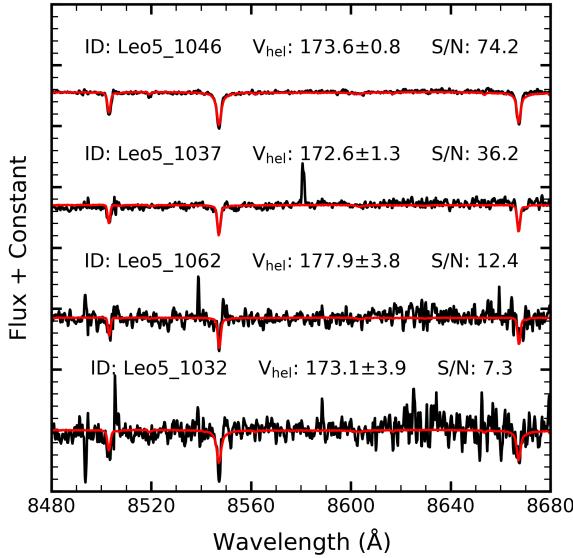
Figure 2. Reduced 1D spectra of four Leo V member stars with varying S/N at wavelength range 8480–8680 Å. The best-fit stellar templates, used to measure radial velocity, are overlaid in red. The resulting velocity measurement (in km s^{-1}) is provided for each spectrum, in addition to its ID and S/N.

While the RFC identifies some poor-fitting stellar templates, it does not find all of them. For this reason, we also discard objects with S/N < 4 or radial velocity uncertainty greater than 20 km s^{-1}. After applying these criteria, we have >1,000 combined stellar observations, including 113 for Boötes I, 95 for Leo IV and 90 for Leo V. Measurements on these stars are reported in Appendix B.

We apply the aforementioned measurements to both the combined spectra as well as the spectra from individual exposures. The former are used for membership determination (§4) as well as the velocity dispersion calculation (§5.2); the latter are used for velocity error correction (§3.2) and binary search (§5.1).

3.2. *Error Correction*

The weighted standard deviation of individual epoch velocities is larger than the corresponding combined radial velocity uncertainty. Therefore, we use the repeat observations to assess the accuracy of our determined radial velocity uncertainties. Following Li et al. (2019), we use a Gaussian mixture model to model the pairwise radial velocity differences $\delta_{i,j} = v_i - v_j$ of stars in the eight UFDs (listed in Table 1) with more than five
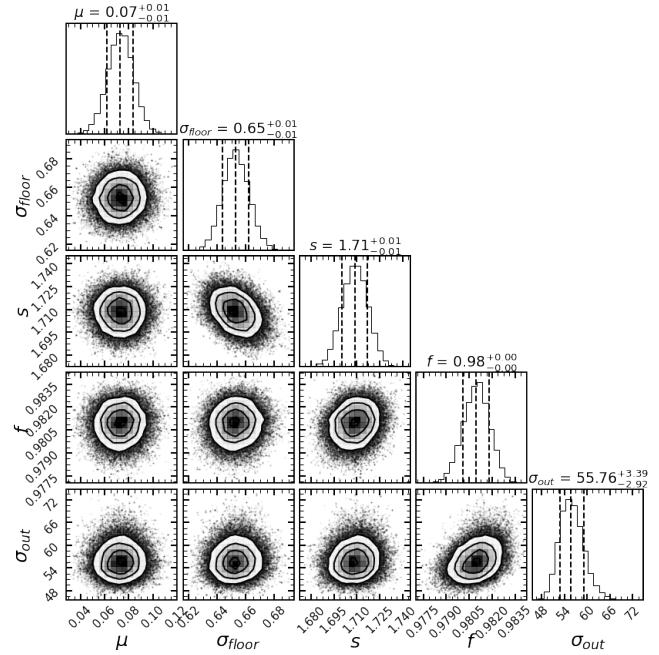

Figure 3. Two-dimensional posterior probability distribution from a MCMC sampler using a five-parameter likelihood for radial velocity uncertainty correction. We use the following parameters: the mean pair-wise radial velocity difference μ, the systematic uncertainty floor σ_{floor}, the uncertainty multiplicative constant s, the fraction of non-outliers f and the outlier standard deviation of pair-wise radial velocity differences σ_{out}.
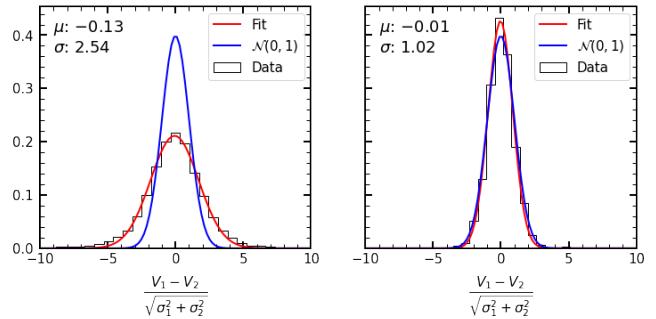

Figure 4. Distribution of 40,165 pairwise radial velocity differences divided by the corresponding corrected uncertainties added in quadrature. The red curve depicts a Gaussian fit to the data and the blue curve depicts a standard normal distribution $\mathcal{N}(0,1)$. The means and standard deviations of the data (computed after applying a five sigma clip) are provided in the top left. Left: Pairwise observations from eight UFDs (with more than five observations each) before correction. Right: Pairwise observations after correction, which approximate a normal distribution $\mathcal{N}(0,1)$.

observations. We have

$$P(\delta_{i,j}) = fN(\delta_{i,j}|0, \sqrt{F(\sigma_i)^2 + F(\sigma_j)^2}) + (1-f)N(0, \sigma_{out})$$
(2)

where N is the Gaussian distribution, σ_i and σ_j are the radial velocity uncertainties corresponding to v_i and v_j, and F corresponds to the uncertainty correction function $F(\sigma) = \sqrt{\sigma_{floor}^2 + (s \times \sigma)^2}$. We only include spectra with S/N > 4 and stars with a radial velocity standard deviation < 20 km s^{-1}. These quality cuts minimize the effect of poor-quality spectra.

We find the scaling factor s and systematic floor σ_{floor} by fitting the model to 3905 radial velocity pairs. We find $s = 1.71$ and $\sigma_{floor} = 0.65$ km s^{-1}, resulting in a final uncertainty correction function:

$$F(\sigma) = \sqrt{0.65^2 + (1.71 \times \sigma)^2}$$
(3)

The posterior probability distributions from the MCMC sampler are displayed in Figure 3. The systematic floor is likely due to the limited accuracy of the wavelength calibration, while the multiplicative constant is likely due to the covariance between pixels in the reduced spectra, as the default GIRAFFE pipeline interpolates the extracted wavelengths to a fixed grid. We compare the original and recalibrated uncertainties in Figure 4 by plotting the distribution of pairwise radial velocity differences divided by the combined uncertainty. The distribution for the recalibrated uncertainties is close to a unit normal distribution, validating our error model. We also apply a similar fit to individual UFDs with more than five observations and obtain similar scaling factors.

3.3. *CaT Metallicity Measurements*

We determine the metallicities using the calcium triplet (CaT) lines at 8400-8700 Å. Following the method described by Li et al. (2019), we fit each CaT line with a Gaussian plus Lorentzian function. The resulting sum provides us with an equivalent width (EW). The EW uncertainty is found from the uncertainty of the fit. In addition, we added a systematic floor of 0.1 Å in quadrature. This was found using the method described in §3.2. The EW is then converted to [Fe/H] using the calibration relation described by Carrera et al. (2013). The metallicity uncertainties are propagated from the CaT EW uncertainties, the photometric uncertainties, distance uncertainties and the uncertainties on the calibration parameters from Carrera et al. (2013).

The calibration relation only applies to red giant stars. Additionally, this approach requires an absolute magnitude measurement, which in turn requires that the distance to the star is known. [Fe/H] calculations are therefore only reliable for UFD member stars. For this reason, we do not provide a metallicity literature comparison for all stars. Instead, we compare the literature and measured metallicity values for Boötes I, Leo IV and Leo V member stars in §5.4, §5.5 and §5.6. All metallicities for stars with S/N less than seven are discarded.

4. MEMBER SELECTION

Although the data processing and measurements described in §2 and §3 are applied to all UFDs in Table 1, we only perform membership selection for Boötes I, Leo IV and Leo V. We will present membership results for the remaining UFDs in a forthcoming paper. We perform membership classification using both subjective evaluation and a mixture model. The subjective classification is used for subsequent velocity and metallicity calculations in §5.

4.1. *Subjective Membership Classification*

We use radial velocity, position, proper motion, metallicity and color-magnitude diagram (CMD) data to evaluate each star's membership subjectively. Location data for each UFD is shown in Figure 6, where we highlight the half-light radii r_h and $\times 3$ half-light radii in black, and mark new and previously identified member stars in green and blue, respectively. We expect member stars to lie close to the center of the galaxies. CMDs using dereddened photometry from DECaLS DR8 are presented in Figure 7. We use a metal-poor ([Fe/H] $= -2.3$) Dartmouth isochrone for identifying red giant branch (RGB) candidates and the M92 blue horizontal branch (BHB) ridgeline for identifying BHB candidates.

Radial velocity and metallicity data are shown in Figure 8. We expect member stars to have a radial velocity within ± 30 km s^{-1} of the UFD's velocity and to have a lower metallicity characteristic of older stars. We therefore classify all stars with inconsistent radial velocities as non-members and refer to non-member stars that have velocities consistent with the UFD as velocity-consistent non-members (VCNMs). We cross-match the VLT observations with the *Gaia* EDR3 catalogue to obtain proper motion and parallax measurements, presented in Figure 9. We expect member stars to have proper motions consistent with the UFD's motion within three standard deviations. Additionally, we exclude foreground stars using a parallax ϖ cut: $\varpi - 3\sigma_\varpi > 0$. For stars with uncertain membership, we visually inspect the Mg I line at 8806.8 Å to determine if the star is a foreground star (Battaglia et al. 2011). This is discussed in Appendix A.

Using these criteria, we identify member stars and VCNMs in the three UFDs, listed in Tables 2, 3 and 4. Finally, we visually inspect the spectra and confirm

that all member stars have qualified measurements on velocity and metallicity fit.

4.2. *Membership Classification via Mixture Model*

We primarily use the above subjective membership selection in §5. In addition, we also compute a membership probability to consider how the Milky Way (MW) foreground properties compare to the UFD and whether the exclusion of this affects our results. This probability is calculated by applying a mixture model to each data set. The mixture model can help justify including or excluding stars on the boundary between the UFD and MW. We use the spatial position, proper motions from *Gaia* EDR3, line-of-sight velocities and metallicities to compute the membership probability.

We model the likelihood with a conditional likelihood to account for the unknown spectroscopic selection function (e.g., Martinez et al. 2011; Horigome et al. 2020):

$$\mathcal{P}(D|R) = f(R)\mathcal{P}_{\mathrm{UFD}}(D|r) + (1-f(R))\mathcal{P}_{\mathrm{MW}}(D|R) \quad (4)$$

with $D = \{v_{\mathrm{hel}}, \mu_{\alpha\star}, \mu_\delta, [\mathrm{Fe/H}]\}$ and $f(R) = \Sigma_{\mathrm{UFD}}(R)/(\Sigma_{\mathrm{UFD}}(R) + \Sigma_{\mathrm{MW}}(R))$. Σ is a 2D density profile. Here v_{hel} is the radial velocity, and $\mu_{\alpha\star}$ and μ_δ are the proper motions. The radial density profile is modeled as a Plummer distribution (Plummer 1911), with best-fit parameters being the projected half-light radii r_h, ellipticity ϵ, and position angle θ. For the spatial parameters (r_h, ϵ, θ) we assume Gaussian priors based on the deeper photometric results from Muñoz et al. (2018). We fix the center to the values in Muñoz et al. (2018). The MW spatial profile is assumed to be constant within the field-of-view of the UFD. We model the velocity and metallicity distributions as Gaussian distributions and the proper motion with a multi-variate Gaussian distribution to account for the correlation between the proper motion terms. As the expected velocity dispersion for a UFD is of order $\sim 5\,\mathrm{km\,s^{-1}}$, which is much smaller than the precision of *Gaia* EDR3 proper motions, we only consider a proper motion dispersion for the MW component. Overall, there are nine parameters to describe the UFD component: $\bar{v}_{\mathrm{hel}}$, σ_v, $\overline{[\mathrm{Fe/H}]}$, $\sigma_{[\mathrm{Fe/H}]}$, $\overline{\mu_{\alpha\star}}$, $\overline{\mu_\delta}$, r_h, ϵ, θ. There are eight parameters to describe the MW component: $\bar{v}_{\mathrm{hel}}$, σ_v, $\overline{[\mathrm{Fe/H}]}$, $\sigma_{[\mathrm{Fe/H}]}$, $\overline{\mu_{\alpha\star}}$, $\sigma_{\mu_{\alpha\star}}$, $\overline{\mu_\delta}$, and σ_{μ_δ}. There is one additional parameter: the relative normalization between the UFD and MW spatial distribution. For the dispersion parameters (e.g., σ_v, $\sigma_{[Fe/H]}$) we assume log uniform priors (also known as Jeffreys priors). The UFD spatial parameters have Gaussian priors and the remaining parameters have uniform priors. To compute membership, we compare
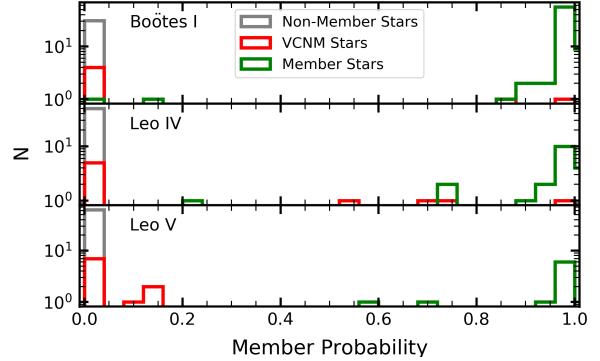

Figure 5. Distribution of Boötes I, Leo IV and Leo V membership probabilities (described in §4), color-coded according to subjective classification. The membership probabilities and subjective classification are largely consistent with each other.

the ratio of the UFD likelihood to total likelihood:

$$P(\mathrm{UFD}|D) = \frac{f(R)P(D|\mathrm{UFD})}{f(R)P(D|\mathrm{UFD}) + (1-f(R))P(D|\mathrm{MW})} \quad (5)$$

To compute the posterior distribution we use the `MultiNest` algorithm (Feroz & Hobson 2008; Feroz et al. 2009). The membership probability (P_m) distributions for each UFD are provided in Figure 5, color coded for different subjectively classified groups: members, non-members and VCNMs. Most members have $P_m > 0.8$ and non-members have $P_m < 0.1$; VCNMs have both high and low membership probabilities. In the following subsections, we discuss in more detail the membership in each UFD and the classification of VCNMs. All measurements, membership probabilities, and subjective membership classifications are given in Appendix B. Mean velocities and metallicities, velocity and metallicity dispersions, and proper motions calculated using the mixture model are listed in Table 5.

4.3. *Boötes I Members*

Using subjective vetting, we identify 69 member stars. Two member stars are assigned a membership probability less than 0.1: Boo1_3 and Boo1_44. Boo1_3's low probability can likely be attributed to its low radial velocity (77.6 ± 6.0 km s^{-1}) while Boo1_44's low probability can be attributed to its high metallicity (-1.22 ± 0.08 dex). Both stars are highlighted in Figures 6, 7, 8 and 9. Because their characteristics are otherwise consistent with being member stars, we subjectively classify them as members. All remaining members have a membership probability greater than 0.8. Additionally, all high-probability stars ($P_m > 0.5$) are classified as members or VCNMs. Two members, Boo1_30 and Boo1_111,

are located high on the RGB. One member, Boo1_32, was previously identified as a c-type RR Lyrae star with a period of 0.3119 days by Dall'Ora et al. (2006), and is therefore excluded from velocity and metallicity dispersions calculations in Section 5.2.

We observe a lack of member stars between g of 17.5 and 19, as seen in Figure 7. This is likely because Boötes I was simulatneously observed with both the GIRAFFE spectrograph and Ultraviolet Visual Echelle Spectrograph (UVES) (Koposov et al. 2011). The bright members at $17.5 < g < 19$ were targeted by UVES, while here we only present the targets observed with GIRAFFE. The lack of bright member stars in the VLT data likely contributes to the proper motion discrepancy discussed in §5.4.

A velocity histogram of all available radial velocities, shown in Figure 10, has a peak at v ≈ 100 km s^{-1}. The Leo IV and Leo V velocity distributions are also shown in Figure 10, and metallicity distributions are provided in Figure 11.

4.4. *Leo IV Members*

We identify twenty Leo IV member stars, including nine new members and eleven members previously identified by Simon & Geha (2007). Our subjective membership selection is largely consistent with our membership probabilities. Only one star, Leo4_1069, is subjectively classified as a member star but assigned membership probability less than 0.5. This is likely due to its lower radial velocity (120.1 ± 2.8 km s^{-1}). Another member, Leo4_1048, is assigned a membership probability of 1.00, but with large uncertainties. This can be attributed to Leo4_1048 having a high metallicity (-1.30 ± 0.15 dex) while having a location and proper motion consistent with being a member star. Additionally, Leo4_1055 is assigned a membership probability of 0.99 but is not classified as a member star because its color-magnitude information is inconsistent with being a Leo IV member.[4] As CMD information is not considered when calculating the membership probability, this inconsistency was not accounted for. Two additional stars with consistent velocities and low metallicities, Leo4_1087 and Leo4_1184, are considered as VCNMs due to inconsistent proper motions and location on the CMD. Simon & Geha (2007) had previously classified Leo4_1087 as a member star.

---

[4] However, Koposov et al. (2018) found a highly carbon-enhanced extremely metal-poor star in Hydrus I that appears to be much redder than the rest Hydrus I members. Therefore, it could possibly be a member star of Leo IV with an unusual chemical abundance pattern.

We measure the velocity of a previously identified RR Lyrae star: Leo4_1041. Moretti et al. (2009) identify Leo4_1041 (called V2 by Moretti et al. (2009) and HiTS113256-003329 by Medina et al. (2018)) as an ab-type RR Lyrae with a period of 0.7096 days.

A velocity histogram of all available velocities (Figure 10) has a peak at v ≈ 130 km s^{-1}. The characteristics of all member stars and VCNMs are given in Table 3.

4.5. *Leo V Members*

We identify eleven Leo V member stars, including four new members, five members previously identified by Walker et al. (2009) and Collins et al. (2017), one RR Lyrae star identified by Medina et al. (2017) and one tentative member identified by Mutlu-Pakdil et al. (2019). One new member star, Leo5_1014, is a BHB star. The remaining three new members are RGB stars. Two of the previously identified members (Leo5_1153 and Leo5_1158) are assigned a membership probability less than 0.2. Leo5_1153 and Leo5_1158 were observed by Walker et al. (2009) and have low membership probabilities because they are far away (∼13 arcmin, >10 r_h) from the center of the galaxy. Mutlu-Pakdil et al. (2019) do not consider these two stars to be members, as the spectra did not pass their quality control cuts and there was no additional information identifying them as members. In this study, we successfully recover their radial velocities and find that they are consistent with Leo V's velocity, suggesting that they could be member stars. If true, this would indicate that Leo V has an extended stellar distribution and support the argument for tidal disruption. However, their metallicity, location and distance from the isochrone are inconsistent with membership, and we therefore do not consider them member stars for subsequent kinematic measurements.

Additionally, one star with a consistent radial velocity and low metallicity, Leo5_1074, is not considered a member due to its distance from the Leo V center. Leo5_1064 similarly has a consistent radial velocity, and is considered a VCNM due to its distance from the Leo V center, distance from the isochrone, and relatively high metallicity. Another star, Leo5_1011, is a BHB star based on its location on the CMD. We classify it as a non-member because we measure its velocity to be 25.1±11.0 km s^{-1} below Leo V's systemic velocity, and no metallicity or proper motion information is available. Furthermore, it is ∼ 0.2 mag brighter than the other BHB member star. Follow-up observations are needed to determine its membership.

We measure a previously identified RR Lyrae star: Leo5_1051. Medina et al. (2017) identify a total of
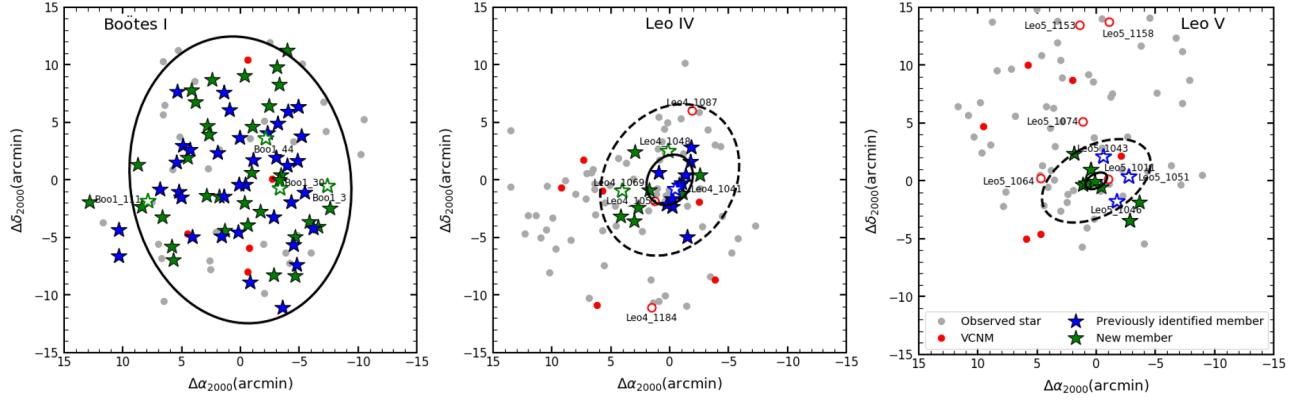
Figure 6. Positional data for Boötes I, Leo IV and Leo V, with r_h and $\times 3\ r_h$ shown in black solid and dotted lines, respectively. Blue stars represent previously identified members while green stars represent new members. Red dots represent velocity-consistent non-members (VCNMs). Dark gray points represent stars with a radial velocity more than 30 km s^{-1} from the UFD's systematic velocity. Open symbols are associated with labels and used for identifying specific stars (see main text for details). The same definitions are used in Figures 7, 8, and 9.
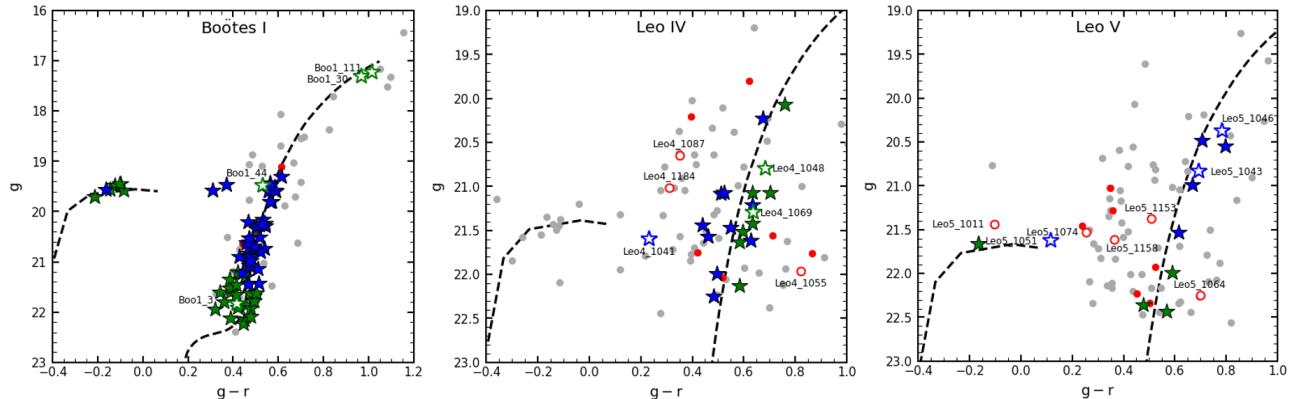

Figure 7. CMD for Boötes I, Leo IV and Leo V, with black dotted lines indicating the M92 BHB ridgeline (Belokurov et al. 2007) and the Dartmouth isochrone with age = 12.5 Gyr and [Fe/H] = −2.3 (Dotter et al. 2008). See Figure 6 for definitions of each symbol.
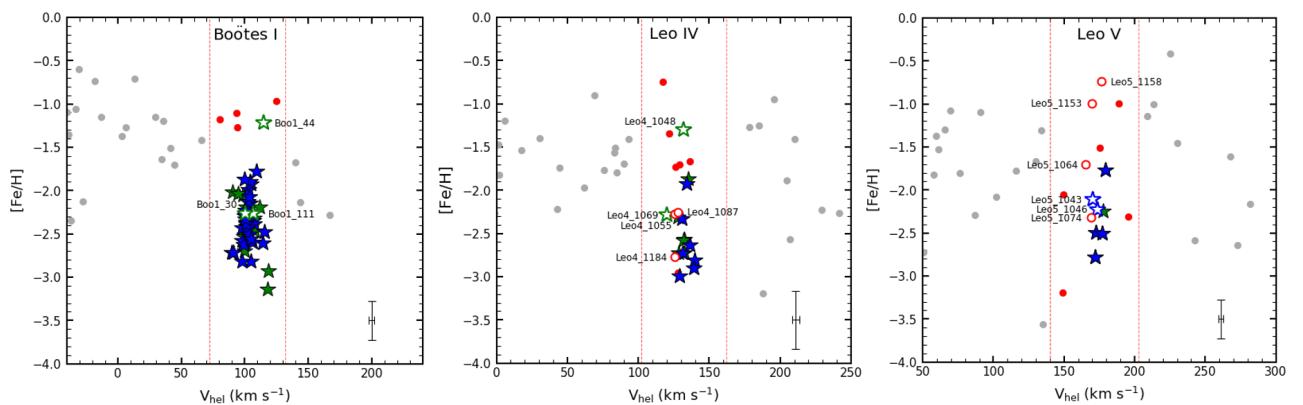

Figure 8. Metallicities and radial velocities for Boötes I, Leo IV and Leo V. We only include stars with reliable measurements for both parameters and therefore do not include BHB or RR Lyrae stars. Red dotted lines indicate the upper and lower bounds placed on radial velocity, defined as 30 km s^{-1} above and below the UFD's systematic velocity. The mean metallicity and radial velocity errors are shown in the bottom right corner of each plot. See Figure 6 for definitions of each symbol.
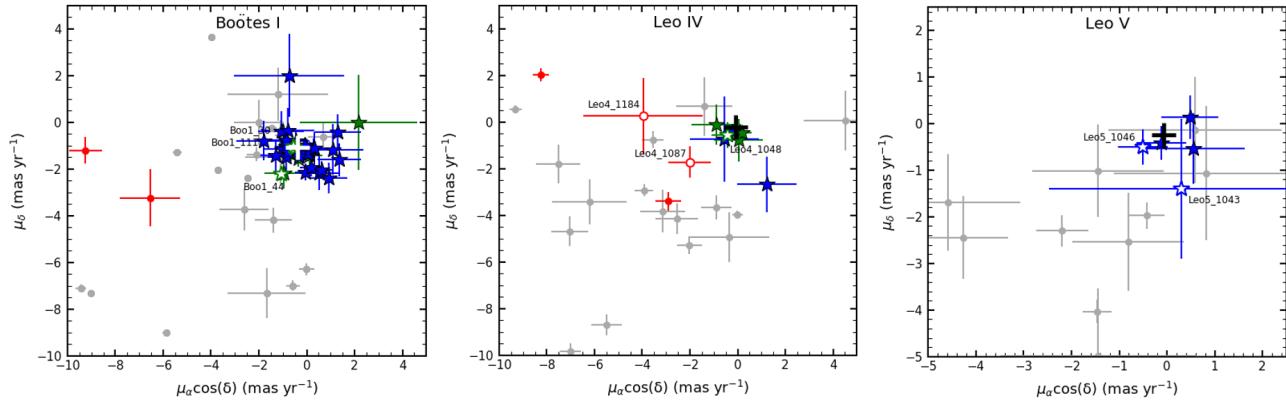
Figure 9. *Gaia* EDR3 proper motions for Boötes I, Leo IV and Leo V. Crosses indicate UFD proper motions from McConnachie & Venn (2020). See Figure 6 for definitions of each symbol.
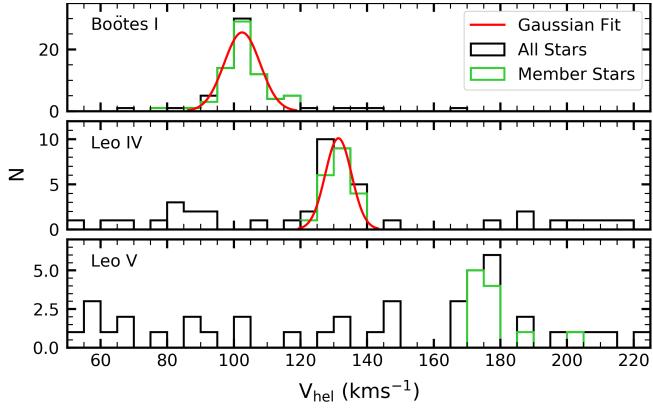
Figure 10. Distributions of all available radial velocities (black histograms) and member star radial velocities (green histograms) for Boötes I, Leo IV and Leo V. Red curves depict a re-scaled Gaussian distribution centered at the derived mean velocity with a standard deviation of the velocity dispersion and median uncertainty added in quadrature. Velocity calculations are described in §5.2. These distributions appear consistent with the distribution of identified members. We note that the Leo V velocity dispersion is not resolved.

three RR Lyrae stars in Leo V, including Leo5_1051 (called HiTS113057+021330 by Medina et al. (2017)), which they classify as an ab-type RR Lyrae with a period of 0.6453 days. Additionally, we identify three stars that Mutlu-Pakdil et al. (2019) listed as plausible Leo V members requiring further follow-up: Leo5_1046, Leo5_1043 and Leo5_1095 (stars 2p, 4p and 3p in Mutlu-Pakdil et al. (2019) Table 10, respectively). Leo5_1046 was previously observed by Walker et al. (2009) but did not pass the quality cuts used by Mutlu-Pakdil et al. (2019). Leo5_1046's radial velocity, proper motion, location, metallicity and color-magnitudes are all consistent with Leo V's characteristics, and we classify it as a member star. Leo5_1043 was identified as a plausible member star because its proper motion and Megacam color-magnitudes were consistent with Leo V. With our spectroscopic data, we confirm that its radial velocity is also consistent, making it another new member star. We find that the final plausible member, Leo5_1095, is not a member, as its radial velocity differs from that of Leo V by almost 200 km s^{-1}.

A velocity histogram of all available velocities (Figure 10) has a peak at v $\approx$ 170 km s^{-1}. The characteristics of all possible members are given in Table 4.

5. DISCUSSION

5.1. *Binarity*

The measured velocity dispersions could be inflated by the presence of binary systems. To investigate this
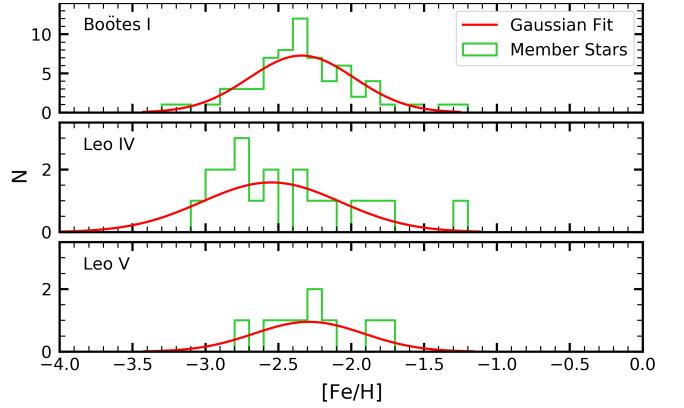

Figure 11. Distributions of all available metallicity measurements for Boötes I, Leo IV and Leo V member stars. Metallicity measurements are described in §3.3 and used in determining membership, as described in §4. Red curves depict a re-scaled Gaussian distribution centered at the derived mean metallicity with a standard deviation of the metallicity dispersion and median uncertainty added in quadrature. Metallicity calculations are described in §5.2.

effect, we measure velocity variation by implementing a χ^2 test on single exposures of the three UFDs. For each star, we measure the single exposure radial velocities using the best-fit stellar template for the combined spectrum. We use 21 exposures for Boötes I, 17 exposures for Leo IV and 17 exposures for Leo V (see §2.1). We perform velocity measurements for single exposures following the same method described in §3.1. Using the null hypothesis that the stellar radial velocity is constant, we calculate a p-value for each member star that has a minimum of two exposures with S/N > 4 and radial velocity uncertainty < 20 km s^{-1}. For stars with a p-value < 0.1, we visually inspect each exposure to verify the quality of our template-fitting radial velocity measurement. This check allows us to discard outliers that are due to noise rather than variability. We then re-calculate the p-value for such stars.

Additionally, both Leo IV and Leo V observations were taken in two groups several months apart. We leverage this to identify potential binary stars by co-adding the spectra taken within each time frame and re-calculating the p-value. This method is especially useful for faint stars that have low S/N from single-exposure spectra.

We can confidently reject the null hypothesis (p<0.01) for one star in Boötes I: Boo1_26. Additionally, we find weak evidence (0.01≤p≤0.1) that three Boötes I member stars exhibit variability: Boo1_61, Boo1_111 and Boo1_114. Three of the four potential binaries (Boo1_26, Boo1_61 and Boo1_111) were assigned a variability probability greater than 0.9 by Koposov et al. (2011) and

Jenkins et al.

Table 2. Properties of Boötes I member stars and VCMNs (stars with radial velocities within ± 30 km s^{-1} of the UFD's velocity). Column (1) is the star ID, the coordinates are given in columns (2) and (3), and column (4) is the r-band magnitude. Columns (5) and (6) are the measured radial velocities and metallicities, respectively. Column (7) provides the membership probabilities described in §4. Uncertainties on the membership probabilities are reported when the uncertainties are larger than 0.01. Column (8) provides the results of our subjective membership selection, including members (indicated by 'M') and VCNMs. The final column contains additional notes. Columns (7) to (9) correspond to columns (8) to (10) in Table 2 and Table 4.

ID	RA	Dec	r	$v_{\rm hel}$	[Fe/H]	P_m	Member	Comments
Boo1_2	209.88958	14.47267	21.44	118.0 ± 5.2	-3.14 ± 0.31	$0.90^{+0.03}_{-0.04}$	M	
Boo1_3	209.89321	14.50475	21.41	77.6 ± 6.0	$--$	$0.14^{+0.10}_{-0.06}$	M	
Boo1_6	209.90667	14.44656	21.05	102.6 ± 4.0	-2.44 ± 0.34	1.00	M	
Boo1_7	209.91400	14.44400	19.73	101.2 ± 1.1	-2.38 ± 0.11	1.00	M	
Boo1_11	209.92575	14.49506	18.91	90.9 ± 0.7	-2.71 ± 0.08	1.00	M	
Boo1_13	209.93100	14.57731	20.16	100.5 ± 1.6	-2.28 ± 0.15	1.00	M	
Boo1_14	209.93575	14.61933	19.75	97.8 ± 1.1	-2.43 ± 0.20	1.00	M	
Boo1_16	209.93729	14.54169	20.20	104.0 ± 1.5	-1.90 ± 0.18	0.99	M	
Boo1_17	209.93775	14.39092	20.62	102.7 ± 2.8	-1.99 ± 0.27	0.99	M	
Boo1_18	209.94046	14.43125	21.70	98.9 ± 7.1	$--$	0.98	M	
Boo1_19	209.94050	14.37525	21.14	90.3 ± 3.7	-2.02 ± 0.38	$0.93^{+0.03}_{-0.04}$	M	
Boo1_21	209.94308	14.41994	19.75	99.3 ± 1.1	-2.62 ± 0.10	1.00	M	
Boo1_22	209.94608	14.48125	20.98	103.5 ± 3.6	-2.07 ± 0.55	1.00	M	
Boo1_24	209.95058	14.61294	20.20	104.4 ± 1.8	-2.14 ± 0.26	1.00	M	
Boo1_25	209.95142	14.53431	19.27	106.8 ± 0.9	-2.32 ± 0.08	1.00	M	
Boo1_26	209.95225	14.70122	19.69	111.5 ± 1.3	-2.19 ± 0.12	1.00	M	Binary star
Boo1_28	209.95888	14.32900	19.63	102.5 ± 1.9	-2.13 ± 0.16	1.00	M	
Boo1_29	209.96146	14.52061	21.12	94.7 ± 4.5	-2.04 ± 0.29	1.00	M	
Boo1_30	209.96212	14.50075	16.33	100.3 ± 0.7	-2.26 ± 0.07	1.00	M	
Boo1_31	209.96283	14.51383	21.48	104.7 ± 5.2	$--$	0.99	M	
Boo1_32	209.96388	14.65161	19.55	113.9 ± 2.2	$--$	1.00	M	RR Lyrae star
Boo1_33	209.96546	14.59536	18.69	100.2 ± 0.7	-2.33 ± 0.07	1.00	M	
Boo1_36	209.96804	14.54600	20.06	100.0 ± 1.9	-1.87 ± 0.18	1.00	M	
Boo1_37	209.97088	14.37558	21.79	102.0 ± 7.8	$--$	0.98	M	
Boo1_38	209.97133	14.45953	20.23	104.9 ± 1.5	-2.56 ± 0.15	1.00	M	
Boo1_39	209.97396	14.51553	19.96	124.7 ± 1.6	-0.97 ± 0.15	0.00	VCNM	Inconsistent proper motion, high metallicity
Boo1_42	209.97871	14.62092	19.55	115.0 ± 2.7	$--$	$0.85^{+0.08}_{-0.14}$	M	BHB star
Boo1_43	209.98054	14.58133	19.00	100.0 ± 0.8	-2.29 ± 0.08	1.00	M	
Boo1_44	209.98325	14.57378	18.95	114.8 ± 0.8	-1.22 ± 0.08	0.00	M	
Boo1_48	209.99104	14.46736	19.85	100.9 ± 1.1	-2.41 ± 0.15	1.00	M	
Boo1_51	210.00100	14.54303	20.00	109.5 ± 1.4	-1.78 ± 0.15	$0.99^{+0.00}_{-0.01}$	M	
Boo1_52	210.00312	14.59139	19.91	119.5 ± 4.1	$--$	1.00	M	BHB star
Boo1_53	210.00412	14.52408	21.29	107.8 ± 4.3	-2.47 ± 0.42	1.00	M	
Boo1_55	210.00638	14.36506	19.24	103.8 ± 0.8	-2.50 ± 0.09	1.00	M	
Boo1_56	210.00692	14.41522	18.49	93.8 ± 0.7	-1.27 ± 0.07	0.00	VCNM	Inconsistent proper motion, high metallicity
Boo1_57	210.00929	14.68728	20.19	80.4 ± 2.2	-1.18 ± 0.18	0.00	VCNM	Inconsistent proper motion, high metallicity
Boo1_58	210.00954	14.44817	21.41	109.0 ± 5.2	$--$	0.99	M	
Boo1_59	210.01017	14.38031	20.56	103.9 ± 2.6	-2.19 ± 0.36	$0.85^{+0.07}_{-0.15}$	VCNM	Inconsistent proper motion
Boo1_60	210.01279	14.50656	20.91	104.8 ± 2.6	-1.92 ± 0.30	1.00	M	
Boo1_61	210.01383	14.48094	20.13	107.2 ± 1.3	-2.32 ± 0.34	1.00	M	Binary star
Boo1_62	210.01450	14.66450	21.18	105.5 ± 5.4	$--$	0.98	M	
Boo1_63	210.02154	14.57439	20.36	104.7 ± 1.8	-2.82 ± 0.27	1.00	M	
Boo1_64	210.02221	14.50647	20.50	100.6 ± 1.9	-2.23 ± 0.22	1.00	M	
Boo1_65	210.02338	14.43856	19.79	105.9 ± 1.1	-2.60 ± 0.11	1.00	M	
Boo1_66	210.03612	14.61508	20.28	102.9 ± 2.2	-2.32 ± 0.16	1.00	M	
Boo1_67	210.04296	14.44072	21.45	101.9 ± 5.5	$--$	0.99	M	
Boo1_68	210.04421	14.63994	19.22	101.1 ± 0.9	-2.37 ± 0.09	1.00	M	
Boo1_69	210.04454	14.49011	18.99	103.9 ± 0.8	-2.28 ± 0.08	1.00	M	
Boo1_70	210.04804	14.43222	20.97	115.6 ± 3.9	-2.48 ± 0.93	$0.98^{+0.01}_{-0.01}$	M	
Boo1_71	210.05096	14.48944	20.79	99.2 ± 2.6	-2.53 ± 0.33	1.00	M	
Boo1_73	210.05383	14.55325	18.87	101.8 ± 0.7	-2.29 ± 0.08	1.00	M	
Boo1_75	210.06112	14.65853	20.85	101.0 ± 3.2	-2.19 ± 0.37	1.00	M	
Boo1_78	210.06588	14.57967	21.22	118.5 ± 6.2	-2.93 ± 0.38	$0.96^{+0.01}_{-0.02}$	M	
Boo1_80	210.06912	14.59167	19.66	100.5 ± 2.3	$--$	1.00	M	BHB star
Boo1_81	210.06925	14.49042	20.74	99.6 ± 2.5	-2.51 ± 0.22	1.00	M	
Boo1_82	210.08579	14.62611	21.62	104.3 ± 6.3	$--$	0.99	M	
Boo1_84	210.09100	14.43147	20.42	89.5 ± 2.2	-2.72 ± 0.23	1.00	M	
Boo1_85	210.09212	14.64394	19.60	99.3 ± 2.3	$--$	1.00	M	BHB star
Boo1_86	210.09350	14.55747	19.09	98.6 ± 0.8	-2.44 ± 0.08	1.00	M	
Boo1_87	210.09721	14.43556	21.27	93.4 ± 4.5	-1.11 ± 0.27	0.00	VCNM	High metallicity
Boo1_88	210.09742	14.54589	21.13	97.7 ± 6.0	$--$	0.99	M	
Boo1_89	210.10483	14.56297	20.41	99.3 ± 1.6	-2.59 ± 0.18	1.00	M	
Boo1_90	210.10625	14.48814	20.47	103.1 ± 2.2	-2.42 ± 0.14	1.00	M	
Boo1_93	210.11075	14.49689	20.60	107.4 ± 1.6	-2.38 ± 0.23	1.00	M	
Boo1_95	210.11267	14.64175	19.72	107.7 ± 3.3	$--$	1.00	M	BHB star
Boo1_96	210.11367	14.53875	19.73	106.5 ± 1.0	-2.35 ± 0.23	1.00	M	
Boo1_98	210.11833	14.39794	20.96	100.0 ± 3.9	-2.70 ± 0.27	0.98	M	
Boo1_100	210.12058	14.41728	21.24	101.3 ± 5.3	-2.33 ± 0.32	1.00	M	
Boo1_108	210.13779	14.49992	19.03	97.6 ± 0.8	-2.81 ± 0.09	1.00	M	
Boo1_111	210.15579	14.48278	16.22	106.9 ± 0.7	-2.26 ± 0.07	1.00	M	Binary star
Boo1_112	210.16483	14.47439	19.71	106.3 ± 3.9	$--$	1.00	M	BHB star
Boo1_114	210.19812	14.40333	20.42	114.1 ± 2.1	-2.60 ± 0.31	1.00	M	Binary star
Boo1_115	210.19821	14.44172	20.77	98.2 ± 2.4	-2.58 ± 0.21	1.00	M	
Boo1_117	210.24133	14.48167	21.26	98.3 ± 4.3	-2.05 ± 0.37	$0.91^{+0.03}_{-0.03}$	M	

Table 3. Properties of Leo IV member stars and VCMNs. See Table 2 for descriptions of columns (1) to (6) and (8) to (10). Column (7) indicates whether the star is a previously identified member (with Mutual = Yes for members that were previously identified).

ID	RA	DEC	r	$v_{\rm hel}$	[Fe/H]	Mutual	P_M	Member	Comments
Leo4_1150	173.17683	−0.68997	19.81	126.2 ± 2.0	−1.73 ± 0.15	No	0.00	VCNM	Inconsistent proper motion, lies far from isochrone, >3 r_h from Leo IV center
Leo4_1051	173.19758	−0.53753	20.44	132.3 ± 2.1	−2.72 ± 0.28	No	1.00	M	
Leo4_1061	173.19867	−0.57681	21.33	145.6 ± 8.0	−−	No	$0.75^{+0.08}_{-0.11}$	VCNM	High v_{hel}, large CaT EW (but low S/N so [Fe/H] is not measured)
Leo4_1087	173.20888	−0.44464	20.29	128.0 ± 2.5	−2.25 ± 0.24	No	$0.71^{+0.09}_{-0.12}$	VCNM	Inconsistent proper motion, lies far from isochrone
Leo4_1057	173.21038	−0.49783	21.49	127.8 ± 4.8	−−	Yes	$0.94^{+0.02}_{-0.03}$	M	
Leo4_1045	173.21108	−0.51897	20.55	139.4 ± 2.2	−2.90 ± 0.11	Yes	$1.00^{+0.00}_{-0.03}$	M	
Leo4_1080	173.21583	−0.62719	20.92	139.9 ± 3.5	−2.81 ± 0.74	Yes	$0.72^{+0.11}_{-0.18}$	M	
Leo4_1039	173.21775	−0.53822	20.98	134.2 ± 2.9	−1.92 ± 0.58	Yes	0.99	M	Binary star
Leo4_1043	173.22304	−0.56425	21.55	128.8 ± 6.1	−−	No	0.98	M	
Leo4_1036	173.22329	−0.54897	21.11	131.7 ± 6.8	−−	Yes	0.99	M	
Leo4_1037	173.22692	−0.55308	20.58	136.2 ± 2.8	−2.63 ± 0.35	Yes	1.00	M	
Leo4_1041	173.23258	−0.55825	21.36	132.4 ± 9.2	−−	Yes	0.99	M	RR Lyrae star
Leo4_1046	173.23729	−0.57222	20.57	129.1 ± 2.1	−2.99 ± 0.25	Yes	1.00	M	
Leo4_1056	173.23750	−0.58386	21.76	125.3 ± 7.4	−−	Yes	$0.95^{+0.02}_{-0.03}$	M	
Leo4_1048	173.24300	−0.50364	20.11	131.8 ± 1.6	−1.30 ± 0.15	No	$1.00^{+0.00}_{-1.00}$	M	
Leo4_1052	173.24458	−0.58056	19.55	131.2 ± 1.0	−2.72 ± 0.12	Yes	1.00	M	
Leo4_1040	173.25583	−0.53419	21.00	130.8 ± 3.2	−2.33 ± 0.24	Yes	1.00	M	
Leo4_1055	173.26150	−0.57553	21.14	125.9 ± 3.7	−2.27 ± 0.23	No	0.99	VCNM	Lies far from isochrone
Leo4_1184	173.26617	−0.73044	20.70	125.7 ± 4.0	−2.77 ± 0.20	No	$0.55^{+0.24}_{-0.34}$	VCNM	Lies off isochrone, >3 r_h from Leo IV center
Leo4_1050	173.26996	−0.55944	20.37	132.2 ± 1.8	−2.57 ± 0.16	No	1.00	M	
Leo4_1065	173.28504	−0.58472	21.05	132.1 ± 3.2	−2.58 ± 0.40	No	0.99	M	
Leo4_1006	173.28958	−0.50436	19.31	128.5 ± 0.9	−2.72 ± 0.11	No	1.00	M	
Leo4_1077	173.29129	−0.60494	20.92	128.2 ± 3.8	−2.31 ± 0.68	No	$0.90^{+0.04}_{-0.05}$	M	
Leo4_1069	173.30796	−0.56075	20.66	120.1 ± 2.8	−2.29 ± 0.25	No	$0.22^{+0.42}_{-0.18}$	M	
Leo4_1085	173.31025	−0.59758	20.79	135.3 ± 3.4	−1.87 ± 0.62	No	$0.76^{+0.08}_{-0.12}$	M	
Leo4_1010	173.33546	−0.56042	19.18	136.3 ± 1.2	−1.67 ± 0.11	No	0.00	VCNM	Inconsistent proper motion
Leo4_1204	173.34379	−0.72672	20.85	121.8 ± 5.0	−1.34 ± 0.34	No	$0.01^{+0.02}_{-0.01}$	VCNM	Lies far from isochrone, >3 r_h from Leo IV center
Leo4_1104	173.36254	−0.51644	20.90	117.2 ± 3.8	−0.74 ± 0.34	No	0.00	VCNM	High metallicity, lies far from isochrone, >3 r_h from Leo IV center
Leo4_1142	173.39346	−0.55628	21.52	107.4 ± 6.8	−−	No	0.00	VCNM	Low v_{hel}, >3 r_h from Leo IV center

were thus considered too variable to include in kinematic measurements. In contrast, Koposov et al. (2011) assigned a variability probability of 0.61 to Boo1_114 and therefore did not classify it as a binary. We visually inspect the single-exposure spectra and confirm that there is distinct velocity variation. It is not used in subsequent kinematics calculations. We do not find evidence of variability for two stars that Koposov et al. (2011) identified as potential binaries: Boo1_30 and Boo1_32. However, Boo1_32 is a previously identified RR Lyrae star and we therefore do not include it in any kinematic calculations. Boo1_30 exhibits a peak-to-peak radial velocity variation of just 2.5 ± 1.7 km s^{-1} and is included in kinematic calculations.

We do not identify any potential binary stars in Leo IV when using single-exposure spectra. However, when we use the two combined spectra, we find that Leo4_1039 exhibits weak evidence of variability, with a p-value of 0.06. We calculate velocities of 141.84 ± 5.46 km s^{-1} and 129.20 ± 4.04 km s^{-1} for the first and second combined observing periods, respectively. This star is too faint to obtain reliable velocity measurements from single-exposure spectra.

We identify one star in Leo V with evidence of variability in velocity (p=0.06) using the combined measurements: Leo5_1034. After investigating the quality

of each exposure, we conclude that Leo5_1034's variability appears to be due to true fluctuations in velocity. Additionally, Mutlu-Pakdil et al. (2019) identified Leo5_1038 as a possible binary. Though we calculate a p-value of 0.57 (single exposures) and 0.11 (combined exposures) for this member, our results are consistent with this claim. As seen in Figure 12, where we compare our measurement to all previous measurements, Leo5_1038's radial velocity appears to change with time. We calculate a weighted standard deviation of 3.22 km s^{-1}, 2.2 times larger than the mean uncertainty of 1.45 km s^{-1}.

We note that although we identify RR Lyrae members in both Leo IV and Leo V, the S/N from single-exposure spectra are too low to derive reliable velocity measurements for velocity variation studies. All potential binaries are displayed in Figure 12.

5.2. Velocity and Metallicity Dispersions

Using our expanded membership catalogues, we recalculate the mean velocities $\bar{v}_{\rm hel}$ and velocity dispersions σ_v for each UFD. We use the two-parameter log-likelihood function from Walker et al. (2009). v_i and σ_i are the measured radial velocity and internal uncertainty, respectively, for the ith of N stars. While σ_i captures the random internal measurement uncertainty, σ_V captures the intrinsic radial velocity dispersion. We assume that the measured radial velocities have a Gaus-
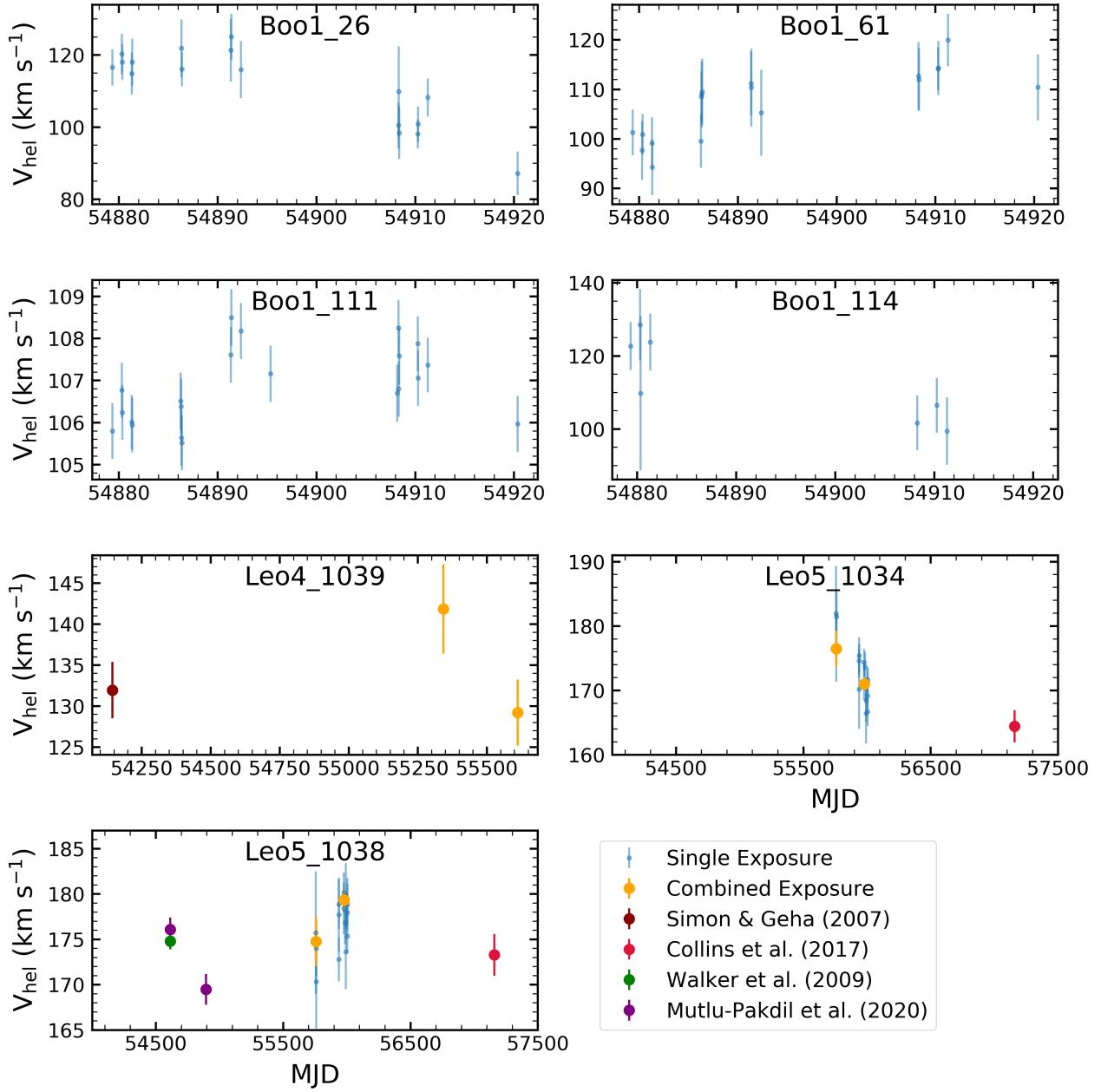
Figure 12. Radial velocities of potential binary stars. We present our single-exposure measurements (blue) and literature radial velocities. Because the Leo IV and Leo V single exposures can be clustered into two groups observed approximately eight and seven months apart, respectively, we separately combine exposures within each observing cluster. The resulting combined radial velocities are shown in orange. Aside from Leo5_1038, all stars show evidence of velocity variation using the VLT measurements alone. Leo5_1038 is a binary found in Mutlu-Pakdil et al. (2019) and our radial velocity measurements support this claim. For Leo4_1039, we are only able to measure its radial velocity from the combined exposures due to the low S/N of single-exposure spectra.

Table 4. Properties of Leo V member stars and VCMNs. See Table 2 for descriptions of columns (1) to (6) and (8) to (10). Column (7) indicates whether the star is a previously identified member (with Mutual = Yes for members that were previously identified).

ID	RA	DEC	r	$v_{\rm hel}$	[Fe/H]	Mutual	P_M	Member	Comments
Leo5_1062	172.72554	2.18881	21.40	177.8 ± 4.4	-2.25 ± 0.63	No	$0.59^{+0.20}_{-0.28}$	M	
Leo5_1069	172.73858	2.16256	20.92	177.1 ± 2.7	-2.50 ± 0.23	Yes	$0.72^{+0.16}_{-0.30}$	M	
Leo5_1051	172.73942	2.22514	21.51	200.3 ± 13.6	$--$	No	$--$	M	RR Lyrae star, high v_{hel}
Leo5_1052	172.75150	2.25575	21.22	195.5 ± 4.9	-2.31 ± 0.70	No	$0.01^{+0.04}_{-0.01}$	VCNM	High v_{hel}
Leo5_1046	172.75692	2.19031	19.58	173.6 ± 0.9	-2.22 ± 0.13	Yes	1.00	M	
Leo5_1158	172.76729	2.44900	21.25	176.5 ± 4.5	-0.74 ± 0.19	No	0.01	VCNM	$>5\ r_h$ from Leo V center
Leo5_1011	172.76917	2.22183	21.54	145.8 ± 10.8	$--$	No	$--$	VCNM	Low v_{hel}, far from BHB ridgeline
Leo5_1043	172.77571	2.25456	20.14	170.1 ± 1.4	-2.11 ± 0.18	No	$0.97^{+0.02}_{-0.08}$	M	
Leo5_1036	172.77850	2.21078	21.88	187.8 ± 6.4	$--$	No	$0.95^{+0.03}_{-0.08}$	M	
Leo5_1032	172.78796	2.21844	21.86	173.3 ± 4.9	$--$	No	0.99	M	
Leo5_1038	172.79412	2.23597	19.75	179.4 ± 1.0	-1.77 ± 0.11	Yes	$1.00^{+0.00}_{-0.06}$	M	Binary star
Leo5_1034	172.80021	2.21656	19.77	171.8 ± 0.9	-2.78 ± 0.10	Yes	1.00	M	Binary star
Leo5_1074	172.80458	2.30533	21.27	169.1 ± 5.3	-2.32 ± 0.61	No	$0.15^{+0.15}_{-0.09}$	VCNM	$>5\ r_h$ from Leo V center
Leo5_1037	172.80500	2.21433	20.32	172.7 ± 1.6	-2.49 ± 0.24	Yes	1.00	M	
Leo5_1153	172.80879	2.44344	20.87	169.7 ± 3.1	-0.99 ± 0.26	No	0.00	VCNM	$>5\ r_h$ from Leo V center
Leo5_1014	172.81762	2.25875	21.83	176.6 ± 13.5	$--$	No	$--$	M	BHB star, $>3\ r_h$ from Leo V center
Leo5_1110	172.81962	2.36503	21.78	141.5 ± 9.8	$--$	No	0.00	VCNM	Low v_{hel}, $>5\ r_h$ from Leo V center
Leo5_1086	172.86425	2.14267	20.93	175.1 ± 4.1	-1.51 ± 0.20	No	$0.14^{+0.15}_{-0.09}$	VCNM	Lies far from isochrone, $>5\ r_h$ from Leo V center
Leo5_1064	172.86454	2.22314	21.55	165.4 ± 5.2	-1.71 ± 0.24	No	$0.09^{+0.15}_{-0.07}$	VCNM	Lies far from isochrone, $>5\ r_h$ from Leo V center
Leo5_1129	172.88267	2.38653	21.84	188.8 ± 6.9	-0.99 ± 0.45	No	0.00	VCNM	High metallicity, $>5\ r_h$ from Leo V center
Leo5_1101	172.88454	2.13583	20.68	149.5 ± 3.0	-2.06 ± 0.33	No	0.00	VCNM	Lies far from isochrone, low v_{hel}, $>5\ r_h$ from Leo V center
Leo5_1124	172.94508	2.29803	21.40	149.3 ± 4.2	-3.20 ± 0.19	No	0.00	VCNM	Low v_{hel}, $>5\ r_h$ from Leo V center

sian distribution centered on $\overline{v}_{\rm hel}$. A uniform prior is used for $\overline{v}_{\rm hel}$. Both a log uniform prior and uniform prior are used for σ_v; we report the former as M1 in Table 5 and the latter as M2. M1 is considered the default value.

The two parameters of interest, $\overline{v}_{\rm hel}$ and σ_V, are estimated by sampling the following distribution:

$$\log \mathcal{L} = -\frac{1}{2} \sum_{i=1}^{N} \ln(\sigma_i^2 + \sigma_V^2) - \frac{1}{2} \sum_{i=1}^{N} \frac{(v_i - \overline{v}_{\rm hel})^2}{(\sigma_i^2 + \sigma_V^2)}. \quad (6)$$

We restrict σ_v to be greater than 0 km s^{-1} and $\overline{v}_{\rm hel}$ to be within the range of member star velocities. We run an MCMC sampler for 5,000 iterations, with a burn-in period of 50 iterations and priors chosen randomly from a normal distribution centered at the member stars' mean velocity. We use a similar approach to determine the mean metallicities $\overline{\rm [Fe/H]}$ and metallicity dispersion $\sigma_{\rm [Fe/H]}$ from our CaT metallicity measurements.

We calculate the mean velocities $\overline{v}_{\rm hel}$, velocity dispersions σ_v, mean metallicities $\overline{\rm [Fe/H]}$ and metallicity dispersions $\sigma_{\rm [Fe/H]}$ of the three dwarf galaxies using the subjectively identified member stars listed in Tables 2-4. For kinematic calculations, we remove potential binary stars and RR Lyrae stars identified in §4 and §5.1, which may potentially inflate the velocity dispersion if included. For metallicity calculations, only bright RGB members are included as we do not have reliable [Fe/H] measurements for horizontal branch stars, nor RGB members with S/N < 7. This results in a total of 64, 18 and 8 members in Boötes I, Leo IV, Leo V in the velocity dispersion calculations and 51, 15 and 7 members in the metallicity dispersion calculations.

The velocity and metallicity dispersions calculated using a log uniform and uniform prior are largely consistent. We do, however, observe a discrepancy in the Leo V velocity dispersion; using a log uniform prior we calculate a dispersion of $0.1^{+1.5}_{-0.1}$ km s^{-1} and using a uniform prior we calculate a dispersion of $2.4^{+2.2}_{-1.6}$ km s^{-1}. Due to the small number of stars included in the calculation, the prior does have an impact to the results. In both cases, we conclude that the Leo V velocity dispersion is not fully resolved. However, when we include the binary stars Leo5_1034 and Leo5_1038, we resolve the velocity dispersion, calculating a value of $3.0^{+1.3}_{-1.0}$ km s^{-1}.

As discussed in §4.3, Boo1_3 has a low membership probability of 0.14 due to its low velocity (more than 20 km s^{-1} below the systemic velocity of Boötes I). Due to its faintness, the proper motion of this star is unavailable; moreover, we are unable to reliably measure its metallicity using the spectrum with S/N = 4. Despite these limitations, we classify it as a member star in the subjective membership classification based on its spatial

location and location on the CMD. We recalculate the velocity dispersion excluding this star and find a slightly lower velocity dispersion of $4.8^{+0.6}_{-0.5}$ km s^{-1}. This is still consistent with the dispersion when the star is included ($5.1^{+0.7}_{-0.8}$ km s^{-1}).

We identify a high metallicity member star in both Boötes I and Leo IV (Boo1_44 and Leo4_1048 with metallicities of -1.22 ± 0.08 and -1.30 ± 0.15 dex, respectively). To evaluate their impact on the metallicity calculations, we re-calculate the mean metallicities and metallicity dispersions without these stars. When excluding Boo1_44, we find no significant difference in the Boötes I mean metallicity, but calculate a lower metallicity dispersion ($0.18^{+0.04}_{-0.03}$ dex, compared to $0.28^{+0.04}_{-0.03}$ dex when including Boo1_44). Additionally, when we exclude Leo4_1048, we calculate a mean Leo IV metallicity of $-2.66^{+0.07}_{-0.07}$ dex (compared to $-2.48^{+0.16}_{-0.13}$ dex when including Leo4_1048). Furthermore, we are no longer able to resolve the Leo IV metallicity dispersion ($0.02^{+0.06}_{-0.01}$ dex) after excluding this star.

For comparison, we also list the velocity and metallicity parameters from the membership probability calculation discussed in §4. This approach uses all stars with good radial velocity and metallicity measurements, as no prior membership or binary information is available before the mixture model analysis is performed. Given the minimal difference in the subjective membership classification and membership probability (Figure 5), these two membership classifications provide similar kinematic and metallicity parameters. However, as stated previously, we obtain different values for the Boötes I metallicity dispersion depending on our treatment of Boo1_44, and we find that our value is only consistent with the dispersion from the membership probability calculation when we exclude this star. This is because the star is assigned a membership probability of zero and so is not considered in the dispersion calculation in the mixture model.

Additionally, while the Leo IV metallicity dispersions are consistent, the mixture model calculates a large uncertainty. This reflects the large uncertainty in Leo4_1048's membership probability ($1.00^{+0.00}_{-1.00}$). Because Leo4_1048 is a member star with a metallicity of -1.30 ± 0.16 dex, its inclusion in metallicity calculations has a large effect on the calculated metallicity dispersion. Just as we are unable to resolve Leo IV's metallicity dispersion when we exclude Leo4_1048 from our member catalogue, the mixture model is unable to resolve the metallicity dispersion when Leo4_1048 is assigned a membership probability of zero.

While we do not resolve the Leo V velocity dispersion, the mixture model calculates a value of $3.2^{+1.7}_{-1.4}$ km s^{-1}.

This is consistent with our value when we include the two binary member stars and is a consequence of the mixture model not excluding binary stars from velocity calculations.

In Figures 10 and 11 we show the velocity and metallicity distribution of all member stars in these three UFDs, overplotted with a Gaussian function centered at the derived mean velocity/metallicity with a standard deviation of the velocity/metallicity dispersion and median uncertainty added in quadrature. Table 5 lists these main properties of the three UFDs.

5.3. Mass-to-Light Ratios

With the new spectroscopically confirmed members, we calculate the mass contained within the half-light radius using the estimator from Wolf et al. (2010):

$$M_{1/2} = 930\sigma_v^2 r_h M_\odot \tag{7}$$

We use the velocity dispersions calculated in §5.2 and the half-light radii measured by Muñoz et al. (2018). The derived dynamical masses $M_{1/2}$ for Boötes I and Leo IV are $4.9^{+1.3}_{-1.2} \times 10^6$ and $1.3^{+0.8}_{-0.8} \times 10^6$ $M_\odot$, respectively. Because the Leo V velocity dispersion is not resolved, we instead compute the 95% upper limit. We calculate the upper limit to be 8.9×10^5 $M_\odot$.

We calculate the luminosity from the V-band magnitudes listed in Table 5. The resulting mass-to-light ratios for Boötes I ad Leo IV are 449^{+251}_{-184} and 315^{+322}_{-222} $M_\odot/L_\odot$, respectively. The 95% upper limit for Leo V is 399 $M_\odot/L_\odot$.

5.4. Boötes I Literature Comparison

Koposov et al. (2011) used an enhanced data reduction pipeline to calculate radial velocities from VLT spectra. They targeted stars that are likely to be members, including nine member stars identified by Muñoz et al. (2006) and 27 member stars identified by Martin et al. (2007). Koposov et al. (2011) observed a total of 118 stars, 100 of which were used for kinematic calculations. Though they consider most of the observed stars to be Boötes I members, they classified 37 of them as highly probable members using the following criteria: low velocity variability, $\log(g) < 3.5$, [Fe/H] < -1.5 and radial velocity error $dv < 2.5$ km s^{-1}.

Because we use the data from the same observations analyzed by Koposov et al. (2011), we expect to measure similar velocities, metallicities and dispersions. Koposov et al. (2011) used 100 stars to calculate the velocity dispersion, and identified a subset of 37 stars as highly probable Boötes I members. We assign a membership probability greater than 0.8 to all Koposov et al. (2011) highly probable members. Of the remaining 36 stars

Table 5. UFD properties from literature are given in the top panel. In the bottom panel, the toal number of member stars identified, used in velocity calculations and used in metallicity calculations are reported, in addition to the updated mean velocities ($\overline{v}_\mathrm{hel}$), velocity dispersions (σ_V), mean metallicities ($\overline{[\mathrm{Fe/H}]}$), metallicity dispersions ($\sigma_{[\mathrm{Fe/H}]}$) and proper motion ($\mu_\alpha\cos(\delta)$, μ_δ). Results are reported for the complete membership catalogue using both log uniform priors (M1) and uniform priors (M2) for dispersion parameters. We consider M1 to be the default values used throughout the study. Additionally, we provide velocity and metallicity values found using the membership probability mixture described in §4.2 (M3).

Parameter		Bootes I	Leo IV	Leo V
RA$_\mathrm{J2000}$ (deg)		210.0200	173.2405	172.7857
Dec$_\mathrm{J2000}$ (deg)		14.5135	-0.5453	2.2194
M$_V$ (mag)		$-6.02^{+0.25}_{-0.25}$	$-4.99^{+0.26}_{-0.26}$	$-4.29^{+0.36}_{-0.36}$
r$_h$ (pc)		191^{+8}_{-8}	114^{+13}_{-13}	49^{+16}_{-16}
Distance (kpc)		$66.0^{+2.0}_{-2.0}$	$154.0^{+5.0}_{-5.0}$	$169.0^{+4.0}_{-4.0}$
$\overline{v}_\mathrm{hel}$ (km s^{-1})		$101.8^{+0.7}_{-0.7}$	$132.3^{+1.4}_{-1.4}$	$170.9^{+2.1}_{-1.9}$
σ_v (km s^{-1})		$4.6^{+0.8}_{-0.6}$	$3.3^{+1.7}_{-1.7}$	$2.3^{+3.2}_{-1.6}$
$\overline{[\mathrm{Fe/H}]}$ (dex)		$-2.35^{+0.09}_{-0.08}$	$-2.29^{+0.19}_{-0.22}$	$-2.48^{+0.21}_{-0.21}$
$\sigma_{[\mathrm{Fe/H}]}$ (dex)		$0.44^{+0.07}_{-0.06}$	$0.56^{+0.19}_{-0.14}$	$0.47^{+0.23}_{-0.13}$
$\mu_\alpha\cos(\delta)$ (mas yr^{-1})		-0.39 ± 0.01	-0.08 ± 0.09	-0.06 ± 0.09
μ_δ (mas yr^{-1})		-1.06 ± 0.01	-0.21 ± 0.08	$-0.25^{+0.09}_{-0.08}$
References[a]		1,1,1,1,2,3,	1,1,1,1,6,7,	1,1,1,1,9,10,
		3,4,4,5,5	7,8,8,5,5	10,10,10,5,5
# of members	Total	69	20	11
	RV	64	18	8
	[Fe/H]	51	15	7
$\overline{v}_\mathrm{hel}$ (km s^{-1})	**M1**	**$102.6^{+0.7}_{-0.8}$**	**$131.6^{+1.0}_{-1.2}$**	**$173.1^{+1.0}_{-0.8}$**
	M2	$102.5^{+0.8}_{-0.7}$	$131.2^{+1.1}_{-1.2}$	$173.5^{+2.0}_{-1.3}$
	M3	$102.9^{+0.7}_{-0.7}$	$131.5^{+1.0}_{-0.9}$	$174.1^{+1.7}_{-1.5}$
σ_V (km s^{-1})	**M1**	**$5.1^{+0.7}_{-0.8}$**	**$3.4^{+1.3}_{-0.9}$**	**$0.1^{+1.5}_{-0.1}$**
	M2	$5.2^{+0.8}_{-0.7}$	$3.5^{+1.4}_{-0.8}$	$2.3^{+2.2}_{-1.6}$
	M3	$5.1^{+0.6}_{-0.5}$	$2.7^{+1.2}_{-1.0}$	$3.2^{+1.7}_{-1.4}$
$\overline{[\mathrm{Fe/H}]}$ (dex)	**M1**	**$-2.34^{+0.05}_{-0.05}$**	**$-2.48^{+0.16}_{-0.13}$**	**$-2.29^{+0.14}_{-0.17}$**
	M2	$-2.34^{+0.05}_{-0.05}$	$-2.48^{+0.18}_{-0.13}$	$-2.30^{+0.17}_{-0.12}$
	M3	$-2.36^{+0.03}_{-0.03}$	$-2.54^{+0.17}_{-0.15}$	$-2.30^{+0.17}_{-0.17}$
$\sigma_{[\mathrm{Fe/H}]}$ (dex)	**M1**	**$0.28^{+0.04}_{-0.03}$**	**$0.42^{+0.12}_{-0.10}$**	**$0.30^{+0.14}_{-0.09}$**
	M2	$0.28^{+0.04}_{-0.04}$	$0.43^{+0.15}_{-0.09}$	$0.34^{+0.17}_{-0.12}$
	M3	$0.14^{+0.04}_{-0.05}$	$0.39^{+0.14}_{-0.33}$	$0.34^{+0.16}_{-0.12}$
$\mu_\alpha\cos(\delta)$ (mas yr^{-1})	M3	$-0.45^{+0.04}_{-0.04}$	$-0.11^{+0.24}_{-0.24}$	$-0.02^{+0.29}_{-0.29}$
μ_δ (mas yr^{-1})	M3	$-1.13^{+0.03}_{-0.03}$	$-0.45^{+0.19}_{-0.19}$	$-0.40^{+0.21}_{-0.21}$

[a]References: (1) Muñoz et al. (2018); (2) Dall'Ora et al. (2006); (3) Koposov et al. (2011); (4) Simon (2019); (5) McConnachie & Venn (2020); (6) Moretti et al. (2009); (7) Simon & Geha (2007); (8) Kirby et al. (2013); (9) Medina et al. (2018); (10) Collins et al. (2017)

with high membership probability, Koposov et al. (2011) disqualified 6 because of their variability, 21 for having a radial velocity error ≥ 2.5 km s^{-1}, 12 for having $\log(g) \geq 3.5$, and 9 for having [Fe/H] ≥ -1.5 (with 11 stars not meeting at least two of the four criteria). Because the Koposov et al. (2011) membership cuts are intended to capture highly probable members, they may be excluding less obvious members. The variability and radial
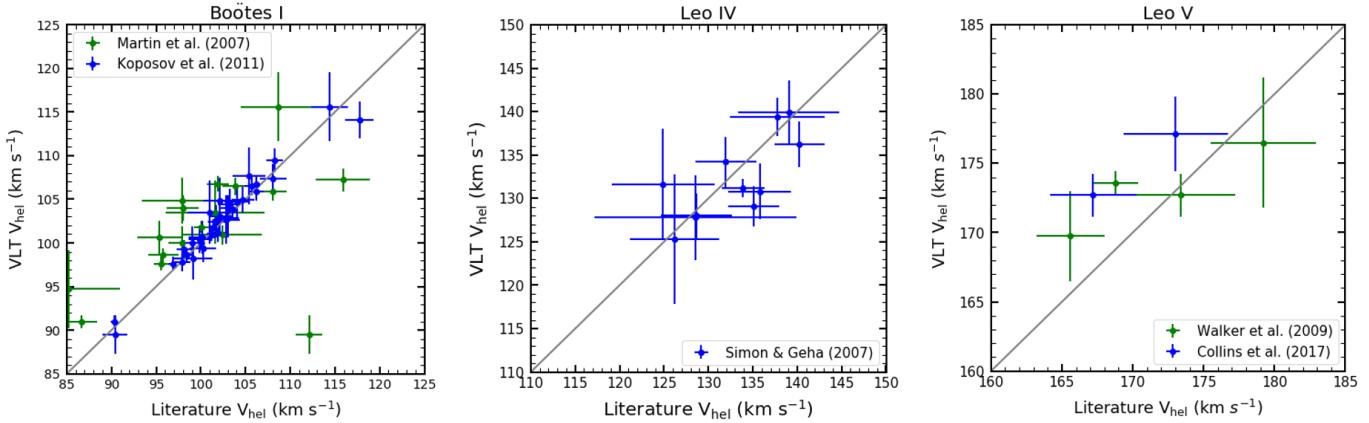
Figure 13. Comparison of Boötes I, Leo IV and Leo V member stars' radial velocity measurements with literature values, excluding binary and RR Lyrae stars. Because there is only one Leo V star (Leo5_1038) in both the VLT data and Mutlu-Pakdil et al. (2019) data with quality spectra, and this star is a binary (see Figure 12), we do not include a comparison with Mutlu-Pakdil et al. (2019). We do not observe a significant offset for either Boötes I or Leo IV. However, for Leo V, we observe a positive offset of 4.8 ± 2.9 km s^{-1} from Collins et al. (2017) based on two common stars.

Figure 14. Comparison of Boötes I, Leo IV and Leo V member stars' metallicity measurements with literature values. Mutlu-Pakdil et al. (2019) observe the same Leo V member star (Leo5_1038) twice; we compare our metallicity to both of their measurements, which differ by 1.31 ± 0.45 dex. This star is considered a binary (see Figure 12).

velocity error cuts in particular may be broadened to capture more members.

We calculate a mean velocity and velocity dispersion of $102.6^{+0.7}_{-0.8}$ and $5.1^{+0.7}_{-0.8}$ km s^{-1}, respectively. These values are consistent with the Koposov et al. (2011) values for a single-component distribution ($\overline{v}_{hel} = 101.8^{+0.7}_{-0.7}$ km s^{-1}, $\sigma_v = 4.6^{+0.8}_{-0.6}$ km s^{-1}). We observe velocity offsets of 0.36 ± 0.37 km and 2.0 ± 1.0 km s^{-1} from Koposov et al. (2011) and Martin et al. (2007), respectively. We compare member stars' velocity measurements to previous literature in the left panel of Figure 13.

Koposov et al. (2011) also fitted a two-component velocity distribution and found a cold component with $\sigma_v \sim 2.4$ km s^{-1} and a hot component with $\sigma_v \sim 9$ km s^{-1}. We fit a similar two component model using a seven parameter likelihood that includes a MW component:

$$P(v) = (1 - f_{MW}) \times (fN(v|\mu, \sigma_1) + (1 - f)N(\mu, \sigma_2)) + f_{MW}N(\mu_{MW}, \sigma_{MW}) \tag{8}$$

μ and μ_{MW} are the mean velocities of Boötes I and MW stars, respectively; σ_1, σ_2, and σ_{MW} are the velocity dispersions of the first Boötes I velocity component, the second Boötes I velocity component, and the MW stars, respectively; and f and f_{MW} are the fraction of Boötes I stars in the first velocity component and the fraction of stars in the foreground, respectively. Using this likelihood, we calculate velocity dispersions ($\sigma_v \sim 2.2$ km s^{-1} and $\sigma_v \sim 9.6$ km s^{-1}) consistent with those found by Koposov et al. (2011). The posterior probability distribution is shown in Figure 15. We also fit a corresponding one component model using a five parameter likelihood (i.e no σ_2 and f).

We compare the models using the corrected Akaike Information Criterion (AICc), which is a likelihood ratio with an additional penalty for the number of model parameters (see Kirby et al. 2013 for details). A smaller AICc value usually corresponds to a more favored model. Our calculated AICc value for the two-component model is lower than one-component model by 3.5, indicating the two-component model is preferred, but with weak evidence.

We calculate a mean metallicity and metallicity dispersion of $-2.34^{+0.05}_{-0.05}$ and $0.28^{+0.04}_{-0.03}$ dex, respectively. The mean metallicity is consistent with the most recent calculation given by Simon (2019). However, our metallicity dispersion is smaller than that from Simon (2019) ($0.44^{+0.07}_{-0.06}$ dex). Koposov et al. (2011) use the best-fit template for each star's co-added spectrum to calculate metallicities. Though their fitting procedure is primarily intended to calculate radial velocities, they find that their resulting values for $T_{\rm eff}$, $\log(g)$ and [Fe/H] are reasonable. We compare our metallicity results with theirs in Figure 14, noting that they do not provide uncertainties for their measurements because of the discreteness of the Munari atmosphere grid (Munari et al. 2005). Assigning their values a uniform uncertainty of 0.3 dex, we find an offset of -0.03 ± 0.06 dex. There is no obvious correlation between our measurements. We also provide a comparison of our results with Martin et al. (2007) and Lai et al. (2011). Measurements from both studies are known to within ± 0.2 dex. We find an offset of -0.47 ± 0.11 and 0.35 ± 0.11 dex relative to the measurements from Martin et al. (2007) and Lai et al. (2011), respectively. This could be attributed in part to the different CaT calibrations used; while we use the calibration relation from Carrera et al. (2013), Martin et al. (2007) use the relation from Rutledge et al. (1997). The comparison results are shown in the left panel of Figure 14.

Using the membership mixture model described in §4.2, we calculate the systematic proper motion in right ascension and declination to be $-0.45^{+0.04}_{-0.04}$ and $-1.13^{+0.03}_{-0.03}$ mas yr^{-1}, respectively. McConnachie & Venn (2020) similarly use the *Gaia* EDR3 catalogue to measure the systematic proper motion of Boötes I, calculating the right ascension and declination components to be -0.39 ± 0.01 and -1.06 ± 0.01 mas yr^{-1}, respectively. The discrepancy between these measurements is likely due to the lack of bright member stars in the VLT data. This is discussed in more detail in §4.3.

5.5. *Leo IV Literature Comparison*

Simon & Geha (2007) used Keck/DEIMOS spectroscopy to identify eighteen Leo IV members. We recover eleven of these stars and identify nine additional members. We calculate a mean velocity and velocity dispersion of $131.6^{+1.0}_{-1.2}$ and $3.4^{+1.3}_{-0.9}$ km s^{-1}, respectively. Simon & Geha (2007) calculated the mean velocity and velocity dispersion using a maximum-likelihood method that assumes a Gaussian velocity distribution, as in Walker et al. (2006). They found values of 132.3 ± 1.4 km s^{-1} and 3.3 ± 1.7 km s^{-1}, respectively. These are consistent with the values calculated using our member catalogue. The Simon & Geha (2007) dispersion is consistent with zero within two standard deviations. Our measurement is therefore the first to resolve the Leo IV velocity dispersion at the 95% confidence level.

The VLT data includes member stars that have previously been identified, providing a source of direct comparison for member velocities. We compare the radial velocity measurements of eleven member stars to previously published findings in the middle panel of Figure 13. We observe that our VLT data for member stars is on average 0.8 ± 2.0 km s^{-1} lower than the literature values. All previously identified members are listed in Table 7 in Appendix C, along with all corresponding velocity measurements.

We calculate a mean metallicity and metallicity dispersion of $-2.48^{+0.16}_{-0.13}$ and $0.42^{+0.12}_{-0.10}$ dex, respectively. These values are consistent with those calculated by Kirby et al. (2013). We compare our calculated metallicities to those measured by Simon & Geha (2007) and Kirby et al. (2013) in the middle panel of Figure 14. We find a mean offset of -0.22 ± 0.17 and -0.17 ± 0.21 dex from Simon & Geha (2007) and Kirby et al. (2013), respectively. The offset from Simon & Geha (2007) is consistent with the difference between the mean metallicities calculated here and by Simon & Geha (2007) (0.16 ± 0.17 dex). This discrepancy can be attributed in part to the different CaT calibrations used. As discussed in §5.4, we use the calibration relation from Carrera et al. (2013), while measurements prior to 2013 use the relation from Rutledge et al. (1997).

Using the membership mixture model, we calculate the systematic proper motion in right ascension and declination to be $-0.11^{+0.24}_{-0.24}$ and $-0.45^{+0.19}_{-0.19}$ mas yr^{-1}, respectively. This is consistent with the values found by McConnachie & Venn (2020).

5.6. *Leo V Literature Comparison*

Walker et al. (2009) identified a total of seven Leo V members observed with MMT/Hectochelle and Collins et al. (2017) performed follow-up with Keck/DEIMOS spectra, finding an additional five members. Mutlu-Pakdil et al. (2019) used photometric data and two epochs of stellar spectra observed with
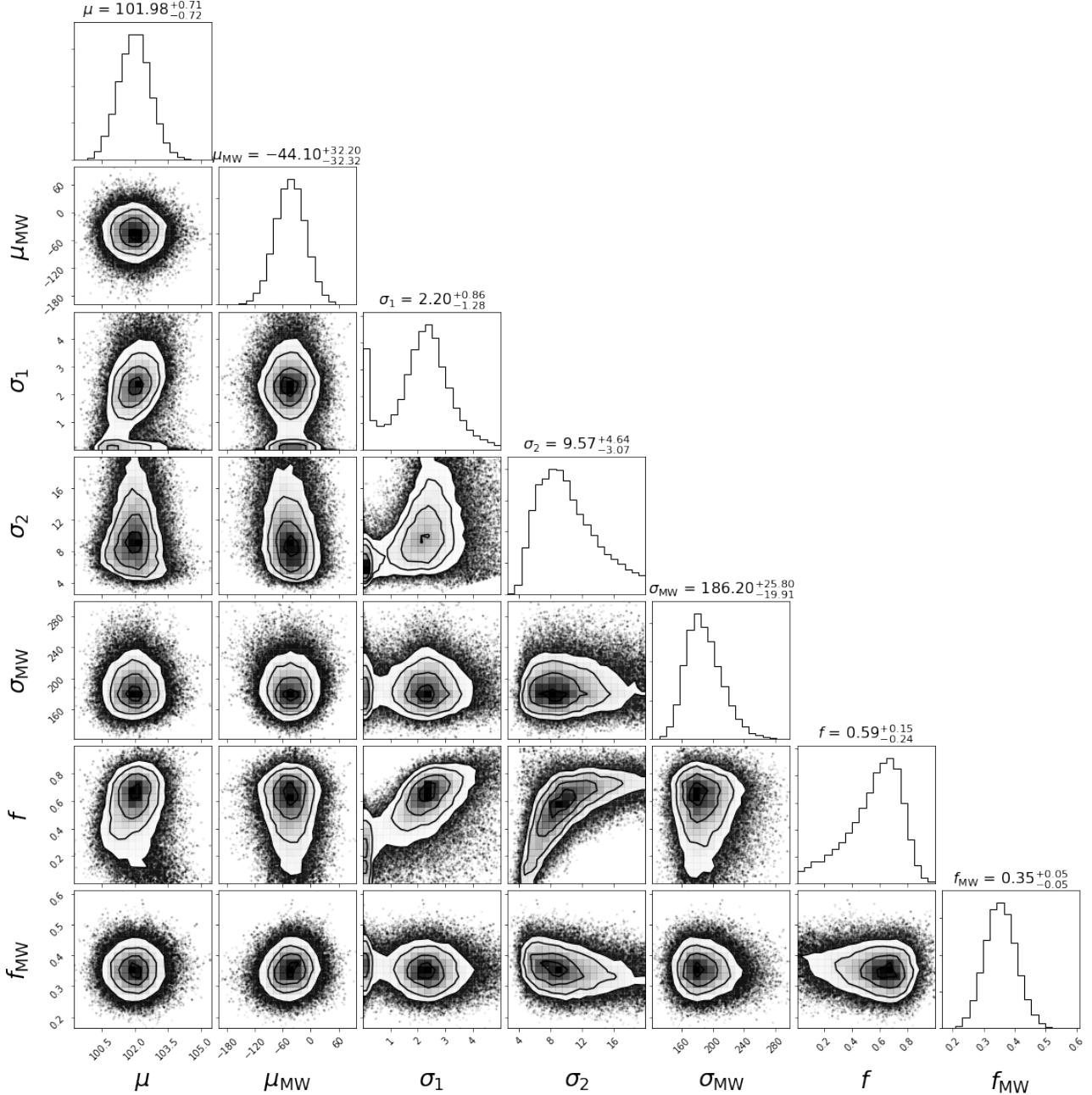
Figure 15. Two-dimensional posterior probability distribution from a MCMC sampler using a seven-parameter likelihood. We use the following parameters: the mean velocity of Boötes I μ, the mean velocity of the foreground MW stars μ_{MW}, the velocity dispersion of the first Boötes I velocity component σ_1, the velocity dispersion of the second Boötes I velocity component σ_2, the velocity dispersion of the MW stars σ_{MW}, the fraction of Boötes I stars in the first velocity component f, and the fraction of MW stars f_{MW}.

MMT/Hectochelle to find three new possible member stars. One of the epochs of spectroscopic data was first reported by Walker et al. (2009). We identify eleven member stars, including four new members, two members previously observed in all three studies, three members observed by Walker et al. (2009) and two members observed by Collins et al. (2017). Walker et al.

(2009) classified two stars (Leo5_1153 and Leo5_1158) located far ($\sim$13 arcmin, >10 r_h) from the center of Leo V as members. These stars are highlighted in Figures 6 through 9. We classify them as VCNMs due to their distance from the Leo V center and their high metallicities.

We calculate a mean velocity of $173.1^{+1.0}_{-0.8}$ km s^{-1} and are unable to resolve the velocity dispersion. Walker

et al. (2009) used a two-dimensional likelihood function weighted by membership probabilities to perform kinematic calculations. Using only the five central members, they found a velocity dispersion of $2.4^{+2.4}_{-1.4}$ km s^{-1}. This value is not conclusively resolved. Including the two distant candidate members increases this value to $3.7^{+2.3}_{-1.4}$ km s^{-1}. Collins et al. (2017) estimated Leo V's kinematics using two models: one that assumes the system is dispersion supported and one that allows for a velocity gradient. For the former, they calculated the mean velocity to be $172.1^{+2.3}_{-2.1}$ km s^{-1} and the velocity dispersion to be $4.0^{+3.3}_{-2.3}$ km s^{-1}; for the latter, they calculated the mean velocity to be $170.9^{+2.1}_{-1.9}$ km s^{-1} and the velocity dispersion to be $2.3^{+3.2}_{-1.6}$ km s^{-1}. Our mean velocity is consistent with the values found by both Walker et al. (2009) and Collins et al. (2017).

We compare the radial velocity measurements of the seven previously identified member stars to published findings in the right panel of Figure 13. Our VLT velocity measurements for member stars are on average 4.8 ± 2.9 km s^{-1} higher than the measurements from Collins et al. (2017) and 1.4 ± 2.1 km s^{-1} higher than the measurements from Walker et al. (2009). Our results for all common stars (members and non-members) are more consistent; we observe 3.4 ± 3.4 km s^{-1} and 0.7 ± 0.9 km s^{-1} offsets from Collins et al. (2017) and Walker et al. (2009), respectively, excluding four common stars with a difference > 100 km s^{-1} from our comparison with Walker et al. (2009). We visually verify the spectra quality for all stars with difference > 100 km s^{-1} and do not identify any poor-quality velocity template fits. All large differences are observed relative to Walker et al. (2009) and could be attributed to Walker et al. (2009) using an older MMT/Hectochelle pipeline that is improved in Mutlu-Pakdil et al. (2019). We measure an offset of 6.6 ± 1.8 km s^{-1} from Mutlu-Pakdil et al. (2019) based on the common binary member star. All previously identified members are listed in Table 8 in Appendix C, along with all corresponding velocity measurements.

We calculate a mean metallicity and metallicity dispersion of $-2.29^{+0.14}_{-0.17}$ and $0.30^{+0.14}_{-0.09}$ dex, respectively. These values are consistent with Collins et al. (2017). We compare our metallicity results to previous literature (Collins et al. (2017) and Mutlu-Pakdil et al. (2019)) in the right panel of Figure 14. The two metallicities from Mutlu-Pakdil et al. (2019) in Figure 14 are calculated from different spectra for the same star. The variability in their results may suggest that their uncertainty is underestimated. The average offset from Collins et al. (2017) is 0.19 ± 0.14 dex.

Using the membership mixture model, we calculate the systematic proper motion in right ascension and declination to be $-0.02^{+0.29}_{-0.29}$ and $-0.40^{+0.21}_{-0.21}$ mas yr^{-1}, respectively. This is consistent with the values found by McConnachie & Venn (2020).

5.7. Metallicity Distribution Function of Boötes I

The VLT data roughly doubles the number of metallicities available in Boötes I compared to the most recent analysis by Lai et al. (2011), bringing it to a total of $\sim$70 stars: 51 in the VLT/GIRAFFE data (29 new stars), and 19 stars in the literature not in our dataset (Norris et al. 2010; Lai et al. 2011). We calibrate the literature measurements to our metallicities using the offset calculated in §5.4.

We re-analyze the metallicity distribution function using three analytic metallicity distribution functions (MDFs) considered by Lai et al. (2011): the leaky box, the pre-enriched leaky box, and the extra gas model (Kirby et al. 2011). The leaky box is the classic analytic model characterized by the effective yield p. The pre-enriched box model adds a minimum metallicity floor $[Fe/H]_0$. The extra gas model (Lynden-Bell 1975) adds pristine gas to a leaky box parameterized by M, where $M = 1$ reproduces the leaky box and $M > 1$ adds extra pristine gas to the leaky box, creating a more peaked MDF with a lighter metal-poor tail. We note that with 41 stars, Lai et al. (2011) found all three models fit the data about equally well, with a slight preference for the extra gas model.

We use dynamic nested sampling with `dynesty` (Speagle 2020) to determine the model parameters and posteriors. The priors are log uniform for p from 10^{-3} to 10^{-1} for all three models; uniform in $[Fe/H]_0$ from -5 to -2 for the pre-enriched model; and uniform in M from 1 to 30 for the extra gas model. The resulting posteriors are all well-behaved. We find $\log p = -2.27 \pm 0.07$ for the leaky box model, $\log p = -2.33 \pm 0.07$ and $[Fe/H]_0 = -3.74 \pm 0.18$ for the pre-enriched box model, and $\log p = -2.32 \pm 0.05$ and $M = 4.5^{+3.2}_{-1.8}$ for the extra gas model. To be consistent with previous similar analyses (Lai et al. 2011; Kirby et al. 2013, 2020) we compare the models using the AICc. Compared to the leaky box model, the pre-enriched model's AICc is 2.9 lower, and the extra gas model's AICc is 6.4 lower. [5] The leaky box model is clearly disfavored, and the extra gas model is slightly preferred over the pre-enriched model. Given that we have the full posterior, a Bayes factor could be

---

[5] Note that in Figure 16 we follow the convention used in Kirby et al. (2013) that a positive ΔAICc corresponds to a lower AICc value compared to the reference AICc.

more appropriate metric to compare these models, but doing so does not change these conclusions.

The new MDF and the results of our fit are shown in Figure 16. The model PDFs have been convolved with the median metallicity uncertainty of 0.22 dex. It is visually apparent that the extra gas model fits the histogram the best. However, the strength of this conclusion relies on including all the literature data. Our VLT/GIRAFFE data alone rule out the pristine leaky box but cannot distinguish between the pre-enriched and extra gas models. This is because the literature data are overall at slightly lower metallicities than the VLT data, increasing the size of the metal-poor tail compared to the peak of the MDF. While we have shifted the mean metallicity of the literature data to match our measurements, it is possible a residual metallicity offset remains, in which case the difference would not be significant. A homogeneous metallicity analysis of Boötes I is needed to be certain.

Taking this result at face value, the MDF suggests that Boötes I was accreting gas, with $M = 4.5^{+3.2}_{-1.8}$ times as much gas being accreted as stars being formed. A similar suggestion has been made by examination of detailed chemical abundances (Frebel et al. 2016), though in that case discrete merging events were responsible rather than continuous gas accretion as modeled here. Regardless, this interpretation is consistent with Boötes I having formed in a similar way to the lowest mass classical dwarf galaxies (Kirby et al. 2011; Yan et al. 2020), emphasizing that relatively massive UFDs like Boötes I are an extension of ordinary galaxy formation to lower stellar masses (Tolstoy et al. 2009; Simon 2019). It remains to be seen if more populated MDFs in lower mass UFDs will continue this trend.

5.8. Leo V Velocity Gradient

Collins et al. (2017) identified a velocity gradient with $\frac{dv}{dx} = -4.1^{+2.8}_{-2.6}$ km s^{-1} per arcmin and a preferred axis of $\phi = 123.6^{+15.5}_{-29.6}$ deg. They argue that this is consistent with disruption caused by tidal interaction with the Milky Way.

We test whether there is a convincing velocity gradient present in the VLT data using a four-parameter model, as in Collins et al. (2017) and Li et al. (2017):

$$\log \mathcal{L} = -\frac{1}{2}\left[\sum_{n=1}^{N}\log(\sigma_{v_{\mathrm{hel}}}^2 + \sigma_{v_i}^2) + \sum_{n=1}^{N}\frac{(v_i - \overline{v}_{\mathrm{hel}} - \frac{dv}{d\chi}\chi_i)^2}{\sigma_{v_i}^2 + \sigma_{v_{\mathrm{hel}}}^2}\right] \quad (9)$$

The parameters of interest are $\overline{v}_{\mathrm{hel}}$, $\sigma_{v_{\mathrm{hel}}}$, velocity gradient $\frac{dv}{dx}$ and position angle of the gradient ϕ. χ_i is the angular distance between the Leo V center (α_0, δ_0) and i-th star (α_i, δ_i) projected to the gradient axis at a

Figure 16. Boötes I MDF. The grey histogram depicts the MDF computed using VLT/GIRAFFE data in combination with the data analyzed by Norris et al. (2010) and Lai et al. (2011). The blue histogram depicts the MDF computed using only GIRAFFE data. The red and blue curves depict the model PDFs using combined data and VLT/GIRAFFE data, respectively. We find that the extra gas model provides the best fit to the combined data.

position angle ϕ:

$$\chi_i = (\alpha_i - \alpha_0)\cos(\delta_0)\sin(\phi) + (\delta_i - \delta_0)\cos(\phi). \quad (10)$$

The posterior probability distributions derived from eight Leo V members (excluding binaries and RR Lyrae members) are displayed on the left side of Figure 17. We find $\frac{dv}{dx} = -0.98^{+0.48}_{-0.50}$ km s^{-1} per arcmin, which is consistent with zero within 2σ uncertainty and is $\sim 4\times$ smaller than the gradient calculated by Collins et al. (2017). Additionally, we find $\phi = 2.4^{+43.7}_{-32.3}$ deg, which is inconsistent with the preferred axis calculated by Collins et al. (2017) ($\phi = 123.6^{+15.5}_{-29.7}$ deg). The weak velocity gradient from the VLT data at a very different preferred axis does not support the significant velocity gradient as seen in Collins et al. (2017); instead, it shows that the inferred gradient from our work is likely due to the small sample used. The discrepancy may also arise in part because Collins et al. (2017) observed a star (StarID-25 in their terminology) at a projected distance of -1.31 arcmin from the center of Leo V and with a radial velocity of 177.8 ± 2.3 km s^{-1}. This star contributed to their observed velocity gradient and was not observed with the VLT. We demonstrate that, along the axis where Collins et al. (2017) find a gradient, the velocities of the VLT members from this work are relatively stable as a function of projected distance in the middle panel of Figure 17. Similarly, along the preferred axis from the VLT data (right panel of Figure 17), we do not observe an obvious trends in the Collins et al. (2017) data.

The weak velocity gradient from the VLT data does not strongly indicate that Leo V is likely on the brink of dissolution, as suggested by Collins et al. (2017). We also note that Leo V's orbit has a large pericenter (168^{+12}_{-104} kpc) (Fritz et al. 2018), which is consistent with there being no tidal disruption. *Gaia* EDR3 will provide updated Leo V orbital information. However, we identify additional nine stars greater than three half-light radii from the center of Leo V that we classify as VCNMs since they are far from the center of the galaxy. Though they exhibit other characteristics inconsistent with membership (e.g. high/low radial velocity, high metallicity, far from isochrone, etc.), if one were to be a member it may be evidence of tidal disruption. A dedicated observation including all known Leo V members from previous literature (16 in total, including three RR Lyrae stars reported by Medina et al. (2017)) and this work is required to further examine the velocity gradient and possible tidal disruption feature in Leo V.

Finally, we caution that such a gradient study is performed on eight member stars which are selected within 30 km s^{-1} of the systematic velocity; this could in principle bias the inferred gradient if the gradient is larger than 10 km s^{-1} per arcmin. However, there is no obvious evidence that such a large velocity gradient exists within the current member catalogue.

6. CONCLUSIONS

Using archived VLT spectroscopic data, we present updated membership catalogues for three UFDs. We summarize our key results for each UFD below:

- **Boötes I:** We identify 69 member stars in Boötes I. Using this membership catalogue, we calculate a systematic velocity of $102.6^{+0.7}_{-0.8}$ km s^{-1}, velocity dispersion of $5.1^{+0.7}_{-0.8}$ km s^{-1}, systematic metallicity of $-2.34^{+0.05}_{-0.05}$ dex and metallicity dispersion of $0.28^{+0.04}_{-0.03}$ dex. Potential binary stars were excluded from all kinematic calculations for Boötes I, Leo IV and Leo V. We measure one member star with a metallicity of -1.22 ± 0.08 dex. When this star is excluded from metallicity calculations, we calculate a metallicity dispersion of $0.18^{+0.04}_{-0.03}$ dex. We find weak evidence in support of the two-component kinematic model used by Koposov et al. (2011), consistent with previous findings. Combining the VLT/GIRAFFE data with data from Norris et al. (2010) and Lai et al. (2011), we re-analyze the Boötes I MDF. We use three distributions from Lai et al. (2011) (leaky box, pre-enriched leaky box and extra gas model) and find that the extra gas model (i.e. a model including infall of pristine gas while the galaxy was

forming stars) best describes the MDF, suggesting that Boötes I formed in a similar way to low mass classical dwarf galaxies. In addition, we find strong evidence that one star (Boo1_26) is a binary and find weak evidence indicating that three stars (Boo1_61, Boo1_111 and Boo1_114) are binary. Koposov et al. (2011) had previously identified three of these stars (Boo1_26, Boo1_61 and Boo1_111) as possible binaries.

- **Leo IV:** We identify 20 member stars in Leo IV, including nine new members. Using this membership catalogue, we calculate a systematic velocity of $131.6^{+1.0}_{-1.2}$ km s^{-1}, velocity dispersion of $3.4^{+1.3}_{-0.9}$ km s^{-1}, systematic metallicity of $-2.48^{+0.16}_{-0.13}$ dex and metallicity dispersion of $0.42^{+0.12}_{-0.10}$ dex. This is the first time the velocity dispersion of Leo IV has been resolved at the 95% confidence level. We measure one member star with a metallicity of -1.30 ± 0.15 dex. When this star is excluded from metallicity calculations, we are unable to resolve the Leo IV metallicity dispersion. In addition, we identify one new possible binary star (Leo4_1039) in Leo IV.

- **Leo V:** We identify eleven member stars in Leo V, including four new members. Using this membership catalogue, we calculate a systematic velocity of $173.1^{+1.0}_{-0.8}$ km s^{-1}, systematic metallicity of $-2.29^{+0.14}_{-0.17}$ dex and metallicity dispersion of $0.30^{+0.14}_{-0.09}$ dex. We also provide further evidence that one Leo V member star (Leo5_1038) is a binary, as suggested by Mutlu-Pakdil et al. (2019), and identify a new possible binary star (Leo5_1034). We do not resolve the velocity dispersion when the two binaries are excluded. We identify a Leo V velocity gradient of $-0.98^{+0.48}_{-0.50}$ km s^{-1} per arcmin, $\sim 4\times$ smaller than the gradient calculated by Collins et al. (2017). The gradient is consistent with zero within 2σ uncertainty and is likely caused by the small sample size. This indicates that Leo V is not tidally disrupted. Additionally, we calculate a preferred kinematic axis that differs from Collins et al. (2017) value by ~ 120 deg.

Because Boötes I contains many (>50) known member stars, including or excluding a small number of plausible members or binary stars does not have a significant effect on the velocity or metallicity dispersion. However, for Leo IV and Leo V (in which only 10-20 members are identified), this could impact the final results. For example, the metallicity dispersion of Leo IV changes
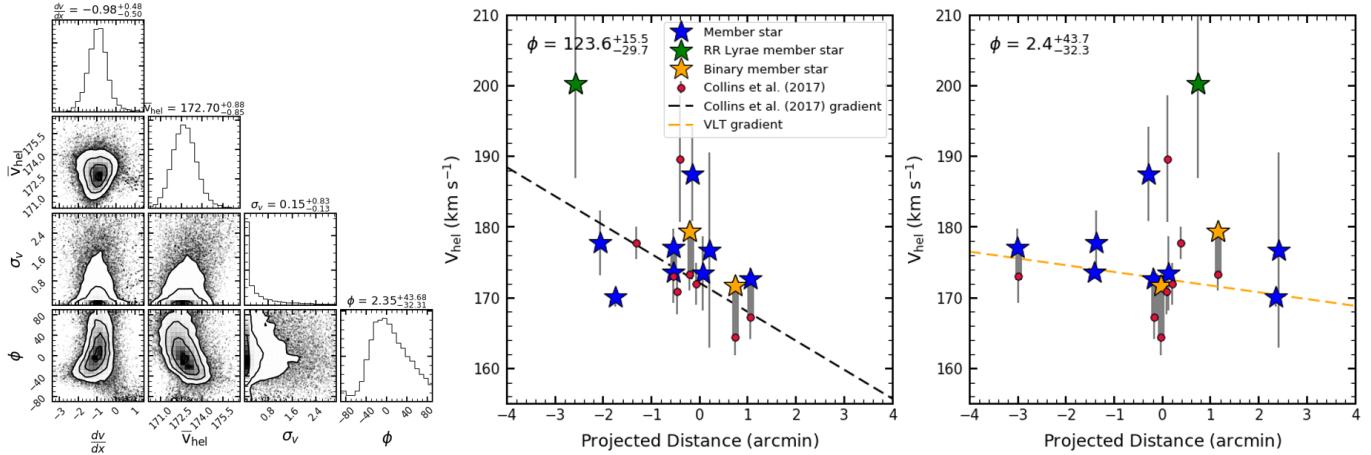
Figure 17. Leo V velocity gradient. Left: Two-dimensional posterior probability distribution from an MCMC sampler using a four-parameter likelihood with the following parameters: systemic velocity $\overline{v}_{\rm hel}$ (km s^{-1}), velocity dispersion σ (km s^{-1}), velocity gradient $\frac{dv}{dx}$ (km s^{-1} per arcmin), and position angle ϕ (deg) over which the velocity gradient is maximised. Middle: The velocities as a function of projected distance along the gradient axis found by Collins et al. (2017). Stars found in both the VLT and Collins et al. (2017) data are located at the same projected distance and are identified by a thick gray line. Our VLT velocity measurements for member stars are on average 4.8 ± 2.6 km s^{-1} higher than the measurements from Collins et al. (2017). The dashed line indicates the velocity gradient found by Collins et al. (2017). The preferred kinematic axis is given in the top left. Right: The velocities as a function of projected distance along the gradient axis found in §5.8. We use the same symbols as used in the middle panel. The dashed line indicates the velocity gradient calculated from the VLT data. The preferred kinematic axis is given in the top left, and differs from the Collins et al. (2017) preferred axis by over 120 deg.

from $0.42^{+0.12}_{-0.09}$ dex to unresolved when one plausible high metallicity member star is excluded, and the velocity dispersion of Leo V becomes unresolved when two binaries are removed from the calculation. For these faint UFDs, more comprehensive observations including all possible bright members are required to better constrain their kinematic and chemical properties.

We provide all spectroscopic measurements and membership results for Boötes I, Leo IV and Leo V in Table 6, with more details on the member stars of each galaxy in Tables 2–4.

This is the first in a series of papers providing consistent, refined measurements of thirteen UFDs using public archival data from VLT/GIRAFFE. Similar spectroscopic analyses for the remaining ten UFDs listed in Table 1 will be presented in forthcoming papers. This series of work will largely improve the sample size of the known UFD member stars for refined kinematic and metallicity property studies on UFDs, provide multi-epoch observations to improve our understanding on the binary stars, and constrain the mass-metallicity relationship in these faintest galaxies.

7. ACKNOWLEDGEMENTS

REFERENCES

Ahnen, M. L., Ansoldi, S., Antonelli, L. A., et al. 2018, JCAP, 2018, 009, doi: 10.1088/1475-7516/2018/03/009

Battaglia, G., & Starkenburg, E. 2012, Astronomy & Astrophysics, 539, A123, doi: 10.1051/0004-6361/201117557

Battaglia, G., Tolstoy, E., Helmi, A., et al. 2011, MNRAS, 411, 1013, doi: 10.1111/j.1365-2966.2010.17745.x

Bechtol, K., Drlica-Wagner, A., Balbinot, E., et al. 2015, ApJ, 807, 50, doi: 10.1088/0004-637X/807/1/50

Belokurov, V., Zucker, D. B., Evans, N. W., et al. 2006, ApJL, 647, L111, doi: 10.1086/507324

—. 2007, ApJ, 654, 897, doi: 10.1086/509718

Belokurov, V., Walker, M. G., Evans, N. W., et al. 2008, ApJL, 686, L83, doi: 10.1086/592962

Blaña, M., Fellhauer, M., & Smith, R. 2012, A&A, 542, A61, doi: 10.1051/0004-6361/201118442

Brown, T. M., Tumlinson, J., Geha, M., et al. 2014, ApJ, 796, 91, doi: 10.1088/0004-637X/796/2/91

Calabrese, E., & Spergel, D. N. 2016, MNRAS, 460, 4397, doi: 10.1093/mnras/stw1256

Carrera, R., Pancino, E., Gallart, C., & del Pino, A. 2013, MNRAS, 434, 1681, doi: 10.1093/mnras/stt1126

Chiti, A., Frebel, A., Ji, A. P., et al. 2018, ApJ, 857, 74, doi: 10.3847/1538-4357/aab4fc

Chiti, A., Frebel, A., Simon, J. D., et al. 2020, arXiv e-prints, arXiv:2012.02309. https://arxiv.org/abs/2012.02309

Collaboration, G., Brown, A. G. A., Vallenari, A., et al. 2020, Gaia Early Data Release 3: Summary of the contents and survey properties. https://arxiv.org/abs/2012.01533

Collins, M. L. M., Tollerud, E. J., Sand, D. J., et al. 2017, MNRAS, 467, 573, doi: 10.1093/mnras/stx067

Dall'Ora, M., Clementini, G., Kinemuchi, K., et al. 2006, ApJL, 653, L109, doi: 10.1086/510665

de Jong, J. T. A., Martin, N. F., Rix, H.-W., et al. 2010, ApJ, 710, 1664, doi: 10.1088/0004-637X/710/2/1664

Dey, A., Schlegel, D. J., Lang, D., et al. 2019, AJ, 157, 168, doi: 10.3847/1538-3881/ab089d

Dotter, A., Chaboyer, B., Jevremovifá, D., et al. 2008, The Astrophysical Journal Supplement Series, 178, 89, doi: 10.1086/589654

Feroz, F., & Hobson, M. P. 2008, MNRAS, 384, 449, doi: 10.1111/j.1365-2966.2007.12353.x

Feroz, F., Hobson, M. P., & Bridges, M. 2009, MNRAS, 398, 1601, doi: 10.1111/j.1365-2966.2009.14548.x

Foreman-Mackey, D., Hogg, D. W., Lang, D., & Goodman, J. 2013, PASP, 125, 306, doi: 10.1086/670067

Frebel, A., Norris, J. E., Gilmore, G., & Wyse, R. F. G. 2016, ApJ, 826, 110, doi: 10.3847/0004-637X/826/2/110

Fritz, T. K., Battaglia, G., Pawlowski, M. S., et al. 2018, A&A, 619, A103, doi: 10.1051/0004-6361/201833343

Fritz, T. K., Carrera, R., Battaglia, G., & Taibi, S. 2019, A&A, 623, A129, doi: 10.1051/0004-6361/201833458

Gaia Collaboration, Prusti, T., de Bruijne, J. H. J., et al. 2016, A&A, 595, A1, doi: 10.1051/0004-6361/201629272

Geha, M., Willman, B., Simon, J. D., et al. 2009, ApJ, 692, 1464, doi: 10.1088/0004-637X/692/2/1464

Gilmore, G., Wilkinson, M. I., Wyse, R. F. G., et al. 2007, ApJ, 663, 948, doi: 10.1086/518025

Hanuschik, R. W. 2003, A&A, 407, 1157, doi: 10.1051/0004-6361:20030885

Hoof, S., Geringer-Sameth, A., & Trotta, R. 2020, JCAP, 2020, 012, doi: 10.1088/1475-7516/2020/02/012

Horigome, S.-i., Hayashi, K., Ibe, M., et al. 2020, MNRAS, 499, 3320, doi: 10.1093/mnras/staa2909

Kennedy, R., Frenk, C., Cole, S., & Benson, A. 2014, MNRAS, 442, 2487, doi: 10.1093/mnras/stu719

Kirby, E. N., Cohen, J. G., Guhathakurta, P., et al. 2013, ApJ, 779, 102, doi: 10.1088/0004-637X/779/2/102

Kirby, E. N., Cohen, J. G., Simon, J. D., & Guhathakurta, P. 2015, The Astrophysical Journal, 814, L7, doi: 10.1088/2041-8205/814/1/l7

Kirby, E. N., Gilbert, K. M., Escala, I., et al. 2020, AJ, 159, 46, doi: 10.3847/1538-3881/ab5f0f

Kirby, E. N., Lanfranchi, G. A., Simon, J. D., Cohen, J. G., & Guhathakurta, P. 2011, ApJ, 727, 78, doi: 10.1088/0004-637X/727/2/78

Koposov, S. E., Belokurov, V., Torrealba, G., & Evans, N. W. 2015a, ApJ, 805, 130, doi: 10.1088/0004-637X/805/2/130

Koposov, S. E., Gilmore, G., Walker, M. G., et al. 2011, ApJ, 736, 146, doi: 10.1088/0004-637X/736/2/146

Koposov, S. E., Casey, A. R., Belokurov, V., et al. 2015b, ApJ, 811, 62, doi: 10.1088/0004-637X/811/1/62

Koposov, S. E., Walker, M. G., Belokurov, V., et al. 2018, MNRAS, 479, 5343, doi: 10.1093/mnras/sty1772

Lai, D. K., Lee, Y. S., Bolte, M., et al. 2011, ApJ, 738, 51, doi: 10.1088/0004-637X/738/1/51

Li, T. S., Simon, J. D., Drlica-Wagner, A., et al. 2017, ApJ, 838, 8, doi: 10.3847/1538-4357/aa6113

Li, T. S., Koposov, S. E., Zucker, D. B., et al. 2019, MNRAS, 490, 3508, doi: 10.1093/mnras/stz2731

Lynden-Bell, D. 1975, Vistas in Astronomy, 19, 299, doi: 10.1016/0083-6656(75)90005-7

Martin, N. F., Ibata, R. A., Chapman, S. C., Irwin, M., & Lewis, G. F. 2007, MNRAS, 380, 281, doi: 10.1111/j.1365-2966.2007.12055.x

Martinez, G. D., Minor, Q. E., Bullock, J., et al. 2011, ApJ, 738, 55, doi: 10.1088/0004-637X/738/1/55

Mau, S., Cerny, W., Pace, A. B., et al. 2020, ApJ, 890, 136, doi: 10.3847/1538-4357/ab6c67

McConnachie, A. W., & Venn, K. A. 2020, arXiv e-prints, arXiv:2012.03904. https://arxiv.org/abs/2012.03904

Medina, G. E., Muñoz, R. R., Vivas, A. K., et al. 2017, ApJL, 845, L10, doi: 10.3847/2041-8213/aa821e

—. 2018, ApJ, 855, 43, doi: 10.3847/1538-4357/aaad02

Moretti, M. I., Dall'Ora, M., Ripepi, V., et al. 2009, ApJL, 699, L125, doi: 10.1088/0004-637X/699/2/L125

Muñoz, R. R., Côté, P., Santana, F. A., et al. 2018, ApJ, 860, 66, doi: 10.3847/1538-4357/aac16b

Munari, U., Sordo, R., Castelli, F., & Zwitter, T. 2005, A&A, 442, 1127, doi: 10.1051/0004-6361:20042490

Muñoz, R. R., Carlin, J. L., Frinchaboy, P. M., et al. 2006, The Astrophysical Journal, 650, L51, doi: 10.1086/508685

Mutlu-Pakdil, B., Sand, D. J., Walker, M. G., et al. 2019, The Astrophysical Journal, 885, 53, doi: 10.3847/1538-4357/ab45ec

Nadler, E. O., Drlica-Wagner, A., Bechtol, K., et al. 2020, arXiv e-prints, arXiv:2008.00022. https://arxiv.org/abs/2008.00022

Norris, J. E., Wyse, R. F. G., Gilmore, G., et al. 2010, ApJ, 723, 1632, doi: 10.1088/0004-637X/723/2/1632

Pasquini, L., Avila, G., Allaert, E., et al. 2000, in Society of Photo-Optical Instrumentation Engineers (SPIE) Conference Series, Vol. 4008, Optical and IR Telescope Instrumentation and Detectors, ed. M. Iye & A. F. Moorwood, 129–140, doi: 10.1117/12.395491

Plummer, H. C. 1911, MNRAS, 71, 460

Rutledge, G. A., Hesser, J. E., & Stetson, P. B. 1997, PASP, 109, 907, doi: 10.1086/133959

Sand, D. J., Strader, J., Willman, B., et al. 2012, ApJ, 756, 79, doi: 10.1088/0004-637X/756/1/79

Schlegel, D. J., Finkbeiner, D. P., & Davis, M. 1998, ApJ, 500, 525, doi: 10.1086/305772

Simon, J. D. 2019, ARA&A, 57, 375, doi: 10.1146/annurev-astro-091918-104453

Simon, J. D. 2019, Annual Review of Astronomy and Astrophysics, 57, 375, doi: 10.1146/annurev-astro-091918-104453

Simon, J. D., & Geha, M. 2007, ApJ, 670, 313, doi: 10.1086/521816

Simon, J. D., Geha, M., Minor, Q. E., et al. 2011, The Astrophysical Journal, 733, 46, doi: 10.1088/0004-637x/733/1/46

Simon, J. D., Drlica-Wagner, A., Li, T. S., et al. 2015, ApJ, 808, 95, doi: 10.1088/0004-637X/808/1/95

Speagle, J. S. 2020, MNRAS, 493, 3132, doi: 10.1093/mnras/staa278

Tolstoy, E., Hill, V., & Tosi, M. 2009, ARA&A, 47, 371, doi: 10.1146/annurev-astro-082708-101650

Walker, M. G., Belokurov, V., Evans, N. W., et al. 2009, ApJL, 694, L144, doi: 10.1088/0004-637X/694/2/L144

Walker, M. G., Mateo, M., Olszewski, E. W., et al. 2015, ApJ, 808, 108, doi: 10.1088/0004-637X/808/2/108

—. 2006, AJ, 131, 2114, doi: 10.1086/500193

Walker, M. G., Mateo, M., Olszewski, E. W., et al. 2016, The Astrophysical Journal, 819, 53, doi: 10.3847/0004-637x/819/1/53

Wolf, J., Martinez, G. D., Bullock, J. S., et al. 2010, MNRAS, 406, 1220, doi: 10.1111/j.1365-2966.2010.16753.x

Yan, Z., Jerabkova, T., & Kroupa, P. 2020, A&A, 637, A68, doi: 10.1051/0004-6361/202037567

Zoutendijk, S. L., Brinchmann, J., Boogaard, L. A., et al.
2020, Astronomy & Astrophysics, 635, A107,
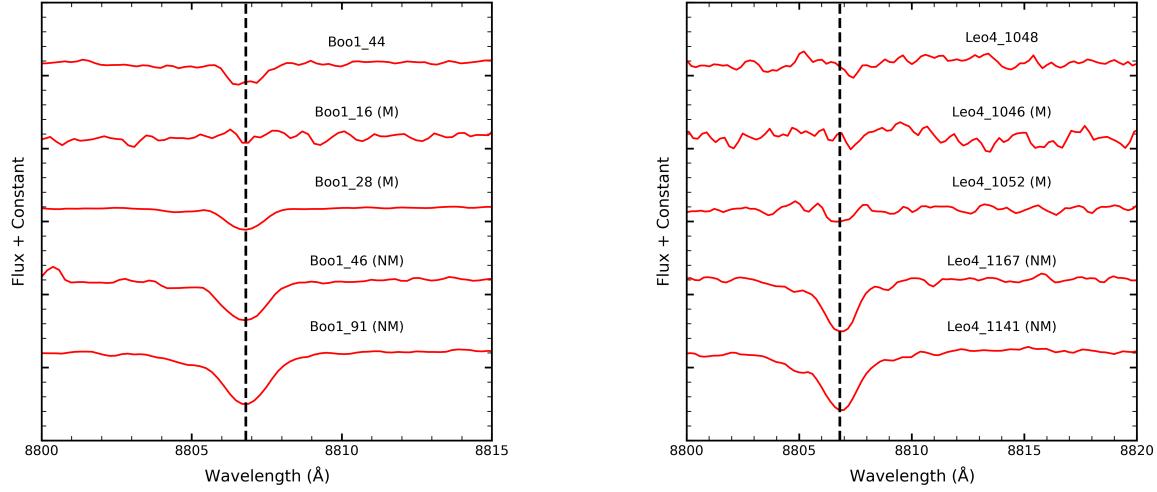doi: 10.1051/0004-6361/201936155

Figure 18. Left: Restframe spectra of the high-metallicity star Boo1_44 centered at the Mg I line, indicated by black dotted line. Spectra of Boötes I member (M) and non-member (NM) stars are shown for comparison. Right: Restframe spectra of the high-metallicity star Leo4_1048. Spectra of Leo IV member (M) and non-member (NM) stars are shown for comparison.

APPENDIX

A. EQUIVALENT WIDTHS OF Mg I LINE AT 8806.8 Å

As shown in Battaglia et al. (2011) and Battaglia & Starkenburg (2012), the Mg I line at 8806.8 Å is gravity sensitive and can be used to discriminate foreground dwarf stars from the giant stars in the dwarf galaxies. We therefore compute the EWs of the Mg I line for all observed stars by integrating the flux over 6 Å around the central wavelength of the line, as was done in Battaglia et al. (2011), and report our measurements in Table 6. Due to the weakness of the Mg I line, it is only visible for bright stars with high S/N. For this reason, we do not use the line for general membership classification. However, the Mg I line is useful for stars with uncertain membership, such as stars with high metallicity but consistent velocity and proper motion, e.g. Boo1_44 ($[Fe/H] = -1.22\pm0.08$) in Boötes I and Leo4_1048 ($[Fe/H] = -1.30\pm0.15$) in Leo IV. In Figure 18, we show the spectra of these two stars centered at the Mg I line, along with several member and non-member stars for comparison. Although Boo1_44 presents a weak Mg I line with an EW of 0.26 ± 0.02, the strength still places it in the "giant" star region as defined by Battaglia & Starkenburg (2012). Leo4_1048 does not show any obvious Mg I line. We therefore conclude that both stars are likely to be giant member stars rather than foreground dwarf stars.

B. ALL OBSERVED STARS

We present radial velocity and metallicity measurements (see §3) for all observed stars in Table 6, in addition to membership probabilities and subjective membership classification (see §4). A portion of the table is shown here to demonstrate its content.

C. MUTUAL STARS

We identify several previously identified member stars in Leo IV and Leo V. Leo IV was previously observed by Simon & Geha (2007). We compare the radial velocities of eleven common member stars in Figure 13 and Table 7. Leo V was previously observed by Walker et al. (2009), Collins et al. (2017) and Mutlu-Pakdil et al. (2019). We compare the radial velocities of seven common member stars in Figure 13 and Table 8.

Table 6. Measurements of all observed stars in Boötes I, Leo IV and Leo V. Only the first four lines are shown. The complete table is available online in a machine readable format. Column (1) is the star ID. Columns (2) and (3) correspond the coordinates and column (4) is the signal-to-noise ratio. Columns (5) and (6) present the radial velocity and CaT equivalent widths described in §3, while column (7) provides the Mg equivalent widths. Column (8) corresponds to the probability calculated using a random forest classifier of the spectrum being good-quality (see §3.1). Column (9) presents the probability of the star being a member (see §4) and column (10) provides the results of our subjective membership classification, with '-1' corresponding to non-member stars and '1' corresponding to member stars.

ID	RA (deg)	DEC (deg)	S/N	$v_{\rm hel}$ (km s^{-1})	CaT EW	Mg EW	GoodstarProb	MembershipProb	Member
Boo1_0	209.8390417	14.6017222	297.40	-13.1±0.7	7.00±0.03	1.11±0.01	0.999	0.0	-1
Boo1_1	209.844125	14.5501944	111.37	140.0±0.7	4.77±0.09	0.2±0.02	1.0	0.0	-1
Boo1_2	209.8895833	14.4726667	7.26	118.0±5.2	0.99±0.20	0.05±0.36	0.999	$0.901^{+0.032}_{-0.043}$	1
Boo1_3	209.8932083	14.5047500	4.42	77.6±6.0	2.86±0.95	0.26±0.6	0.977	$0.143^{+0.103}_{-0.063}$	1

Table 7. Properties of previously identified Leo IV member stars. The Simon & Geha (2007) IDs and radial velocity measurements are distinguished by SG.

RA (deg)	Dec (deg)	ID	$v_{\rm hel}$ (km s^{-1})	ID$_{SG}$	v$_{SG}$ (km s^{-1})	Comments
173.208875	−0.4446389	Leo4_1087	128.0 ± 2.5	383_212	128.65 ± 3.99	
173.210375	−0.4978333	Leo4_1057	127.8 ± 4.8	383_688	128.52 ± 11.38	
173.2110833	−0.5189722	Leo4_1045	139.4 ± 2.2	383_262	137.8 ± 5.32	
173.2158333	−0.6271944	Leo4_1080	139.9 ± 3.5	383_708	139.05 ± 5.68	
173.21775	−0.5382222	Leo4_1039	134.2 ± 2.9	383_715	131.95 ± 3.45	Binary star
173.2232917	−0.5489722	Leo4_1036	131.7 ± 6.8	383_738	124.91 ± 5.76	
173.2269167	−0.5530833	Leo4_1037	136.2 ± 2.8	383_266	140.24 ± 2.8	
173.2325833	−0.55825	Leo4_1041	132.4 ± 9.2	383_269	118.34 ± 7.36	RR Lyrae star
173.2372917	−0.5722222	Leo4_1046	129.1 ± 2.1	383_393	135.12 ± 2.89	
173.2375	−0.5838611	Leo4_1056	125.3 ± 7.4	383_391	126.22 ± 5.02	
173.2445833	−0.5805556	Leo4_1052	131.2 ± 1.0	383_229	133.88 ± 2.41	
173.2558333	−0.5341944	Leo4_1040	130.8 ± 3.2	384_278	135.79 ± 3.51	

Table 8. Properties of previously identified Leo V member stars. The Walker et al. (2009) IDs and radial velocity measurements are distinguished by W, the Collins et al. (2017) values are distinguished by C and the Mutlu-Pakdil et al. (2019) values are distinguished by MP.

RA (deg)	Dec (deg)	ID	$v_{\rm hel}$ (km s^{-1})	ID$_W$	v$_W$ (km s^{-1})	ID$_C$	v$_C$ (km s^{-1})	ID$_{MP}$	v$_{MP}$ (km s^{-1})	Comments
172.794125	2.2359722	Leo5_1038	179.4 ± 1.0	L5−002	174.8 ± 0.9	StarID−37	173.26 ± 2.3	LeoV−6	176.1 ± 1.3, 169.5 ± 1.7	Binary star
172.805	2.2143333	Leo5_1037	172.7 ± 1.6	L5−001	173.4 ± 3.8	StarID−43	167.21 ± 3.1	..	...	
172.7385833	2.1625556	Leo5_1069	177.1 ± 2.7	..	..	StarID−17	173.02 ± 3.7	..	...	
172.8002083	2.2165556	Leo5_1034	171.8 ± 0.9	..	..	StarID−41	164.44 ± 2.5	..	...	Binary star
172.7569167	2.1903056	Leo5_1046	173.6 ± 0.9	L5−007	168.8 ± 1.6	..	..	..	...	
172.7672917	2.449	Leo5_1158	176.5 ± 4.5	L5−057	179.2 ± 3.7	..	..	..	...	
172.8087917	2.4434444	Leo5_1153	169.7 ± 3.1	L5−052	165.6 ± 2.4	..	..	..	...	